New Insights Into the Mechanisms of Signal Formation in RF-Spoiled Gradient Echo Sequences

Vincent Denolin,[1] Céline Azizieh,[2] and Thierry Metens[1]

RF spoiling is a well established method to produce T_1-weighted images with short repetition-time gradient-echo sequences, by eliminating coherent transverse magnetization with appropriate RF phase modulation. This paper presents 2 novel approaches to describe signal formation in such sequences. Both methods rely on the formulation of RF spoiling as a linear increase of the precession angle between RF pulses, which is an alternative to the commonly used quadratic pulse phase scheme. The first technique demonstrates that a steady state signal can be obtained by integrating over all precession angles within the voxel, in spite of the lack of a genuine steady-state for separate isochromats. This clear mathematical framework allows a straightforward incorporation of off-resonance effects and detector phase settings. Moreover, it naturally introduces the need for a large net gradient area per repetition interval. In the second step, a modified partition method including RF spoiling is developed to obtain explicit expressions for all signal components. This provides a physical interpretation of the deviations from ideal spoiling behavior in FLASH and echo-shifted sequences. The results of the partition method in the small flip angle regime are compared with numerical simulations based on a Fourier decomposition of magnetization states. Measurements performed with in vitro solutions were in good agreement with numerical simulations at short relaxation times ($T_1/TR = 32$ and $T_2/TR = 4$); larger deviations occurred at long relaxation times ($T_1/TR = 114$ and $T_2/TR = 82$). Magn Reson Med 54:937–954, 2005. © 2005 Wiley-Liss, Inc.

Key words: fast imaging; gradient echo; RF spoiling; steady-state; partition method; echo shifting

The introduction of gradient echo techniques in MR imaging has dramatically reduced scan times through the use of very short repetition times, combined with low flip angles to limit the spin system saturation. The clinical impact of this acceleration has been considerable in terms of patient comfort, motion artifact reduction, and new applications, such as cine imaging of the heart or contrast-enhanced MR angiography. However, the price paid for this is an increased complexity of signal formation mechanisms, which makes it difficult to characterize and control the contrast behavior of fast gradient echo sequences.

At long repetition times ($TR \gg T_2$) the transverse magnetization vanishes irreversibly between consecutive pulses; hence, the signal intensity is determined solely by the balance between longitudinal magnetization reduction due to

RF pulses and T_1 recovery between pulses. In the steady-state, these two mechanisms compensate each other, leading to the well-known Ernst formula for signal intensity (1–3). At very short echo-time this expression depends only upon the flip angle, T_1, and the repetition time, leading to a purely T_1-weighted contrast. The signal is maximized at $\alpha = \alpha_E = \arccos(E_1)$ (Ernst angle) where α is the flip angle and $E_1 = \exp(-TR/T_1)$. When TR becomes comparable or shorter than T_2, the remaining transverse magnetization at the end of each repetition can no longer be neglected, even when a strong gradient spoiler is placed at the end of each repetition interval. Indeed, successive RF pulses are capable of partly refocusing the magnetization, leading to spin, stimulated and higher order echoes. If the amplitude and phase of RF pulses and the net gradient area per TR are maintained constant along the sequence, the resulting steady-state signal intensity is proportional to T_2/T_1 (2); hence, the image contrast is generally sub-optimal since this ratio is less differentiated than the relaxation parameters themselves. For this reason, several strategies have been developed that break the periodicity in order to "spoil" the coherent magnetization at the end of each repetition interval, as an attempt to restore the contrast properties of long-TR gradient echo techniques. A first approach, known as gradient spoiling, consisted of linearly varying the net gradient area per repetition interval (4,5). The major drawback of this technique was the spatial dependence of the net precession angle between pulses, giving rise to bands with different signal intensities in the image if the phase encoding gradient was used (4) or signal variations from slice to slice if the varying gradient was set along the slice selection direction. As already suggested by Crawley and coworkers (4) and experimentally demonstrated by Zur and colleagues (6), a solution for this problem consists of substituting the varying net gradient area per TR with a linear increase of the interpulse precession angle or, equivalently, a quadratic variation of the RF and detector phases. Rapidly this second approach, known as RF spoiling, has appeared to be a robust and efficient solution for short-TR T_1-weighted gradient-echo imaging. It is presently available on all clinical scanners.

Since the introduction of RF spoiling, several groups have conducted theoretical studies to characterize signal formation in such sequences. Most often the problem has been studied with numerical simulations, either by calculating the magnetization time course for a large number of isochromats and summing the resulting vectors (5–8) or, more recently, by formulating the problem as the calculation of Fourier coefficients (9). Using these techniques, it was possible to verify that the signal intensity reaches a steady state, and to assess the influence of various parameters, including flip angle, relaxation times, and precession angle increment. Namely, high steady-state signals were found for increments of the form $(K/P)(2\pi)$, with K

and P integer. Since numerical results are not easily generalized and do not provide much intuition about the physical origins of the observed behavior, more qualitative descriptions have been developed as well. These were based either on the assessment of phase accumulation along magnetization pathways (6) or approximations using Fourier analysis and analogies with BURST sequences (8). Finally, in Ref. (10), analytical calculations have been conducted to derive a steady-state Fourier expansion of the transverse magnetization and to evaluate the Fourier coefficients for precession angle increments of the above-mentioned form.

The present article brings additional elements to the theoretical understanding of RF-spoiled gradient echo sequences. The first part of the article presents a new approach to solve the apparent paradox that, although RF spoiled sequences are non-periodical, a steady-state signal intensity can be established after a sufficient number of TR intervals. By formulating the problem in terms of linearly increasing precession angles instead of quadratically increasing RF phase, we show that individual spins inside a voxel do not reach a steady state, but integrating over all possible precession angles in a voxel makes it possible to obtain a stationary signal intensity. This formulation offers several advantages, among which are a great mathematical simplicity, the ability to incorporate off-resonance effects, and a straightforward explanation of why a large net gradient area per repetition interval is needed. In the second part, more physical insight into the mechanisms of signal formation is gained by expressing the RF-spoiled signal intensity as a superposition of gradient, spin, and stimulated echoes, using the partition method introduced initially by Kaiser and colleagues (11). This technique has already been suggested as a qualitative or semi-quantitative description of RF-spoiled sequences (2,3,6), but our goal is to derive explicit expressions for all magnetization components in order to quantify their interference as functions of the precession angle increment. In the small flip angle limit, this allows us to give a physical interpretation of the peaks observed in the graph of signal intensity versus precession angle increment. Also, the partition method provides an interpretation of deviations from the ideal spoiling behavior assumed previously for echo-shifted sequences (12). In this sense, the present study can be considered as an extension of Ref. (13), dealing with coherent (i.e., non-spoiled) echo-shifted sequences. Numerical simulations based on the calculation of Fourier coefficients of the magnetization during the approach towards steady state (2,9,14) are used to assess the accuracy of signal intensities obtained with the partition method in the small flip angle limit. Finally, the theoretical findings are confirmed by in vitro experiments, and the links with previous publications on this subject are discussed.

THEORY

The sequence structure considered in this paper is sketched in Fig. 1. RF pulses are applied at a rate of 1 per TR and rotate the magnetization by α about the x axis. The peak of the echo signal (or the origin of k-space in the readout direction) occurs at time TE after each RF pulse. Between pulses the magnetization vector precesses by θ under the effect of ap-
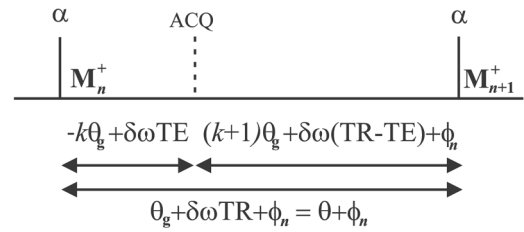
FIG. 1. Schematic view of spoiled gradient-echo sequences. Each RF pulse rotates the magnetization vector by α around the x axis. During the delay TE between the n-th excitation and the n-th readout, the magnetization vector experiences a precession angle of $-k\theta_g$ due to applied gradients and $\delta\omega TE$ as a consequence of permanent off-resonance effects, such as field inhomogeneity or chemical shift. During the second part of the repetition interval, that is, the delay $TR-TE$ between the n-th excitation and the $(n+1)$-th excitation, the magnetization precesses by $(k+1)\theta_g$ due to applied gradients, and $\delta w(TR-TE)$ as a consequence of permanent off-resonance effects. Spoiling is achieved by adding a variable precession angle ϕ_n at the end of each repetition interval. FLASH corresponds to $k = 0$, and echo-shifted sequences to $k = 1$. The magnetization vector just after the n-th RF pulse is noted $\mathbf{M}_n^+$.

plied magnetic field gradients and permanent off-resonance effects (such as field inhomogeneity or chemical shift), and ϕ_n as a consequence of RF spoiling.

For a reason that will be clarified later, we consider only sequences with a "large" net gradient area per TR (i.e., inducing a phase spread larger than 2π across a voxel). This area is kept constant along the sequence, that is, the gradient-induced precession angle, noted θ_g, is the same in all repetition intervals. This implies that phase encoding gradients are properly rewound. Since the slice thickness is generally larger than the in-plane voxel size, setting the uncompensated gradient along the slice-selection direction is usually less demanding than in plane directions in terms of gradient performance. Given these constraints, different contrasts can be generated by varying the amount of gradient-related precession occurring before and after the signal acquisition, noted $-k\theta_g$ and $(k+1)\theta_g$, respectively. The most common option consists of directly sampling the free induction decay (FID) generated after each pulse ($k = 0$); this is usually referred to as GRASS or N-FFE in the coherent case, and (spoiled) FLASH, spoiled GRASS, T1-FFE, or SPGR in the spoiled version (2,10). Setting the large uncompensated gradient before the echo, rather than at the end of the repetition interval, yields the so-called CE-FAST (15), PSIF, or T2-FFE (2) sequence ($k = -1$). TR-shifted echoes (16,17), or ES-FFE sequences (13), are generated when the gradient area before data sampling is taken to be the opposite of the net gradient area per TR ($k = +1$), and consequently the gradient area after echo collection is 2 times the total gradient area ($k + 1 = 2$). More generally, several echoes with various coherence orders (i.e., different k values) can be produced in each repetition interval (18−21).

Permanent off-resonant effects are characterized by their frequency offset $\delta\omega$, leading to a precession angle of $\delta\omega TE$ between the RF pulse and the acquisition window center, and $\delta\omega(TR - TE)$ between the readout and the end of the repetition interval. Flow and diffusion effects are not considered in this article.

Spoiling is achieved by introducing an additional precession angle ϕ_n which occurs after data acquisition, is position-independent, and increases linearly with the pulse index n:

$$\phi_n = \phi_0 + n\psi. \qquad [1]$$

The detector phase is set to $k\phi_{n-1}$ to ensure that the signal reaches a steady state both in amplitude and in phase, as demonstrated below. Note that our formulation, involving invariant RF pulse phases and linearly increasing precession angles, is not a direct representation of the most common implementation of RF spoiling, that is, a quadratic pulse phase variation combined with a detector phase set to that of the $(n - k)$-th pulse. The equivalence between both approaches, which was already mentioned in Ref. (6) in the case of $k = 0$, is proved formally in Appendix A. Our formulation was chosen for its mathematical simplicity and the resulting ease of interpretation.

Pseudo-Steady State for Local Magnetization Vectors

For a fixed value of the precession angle θ due to gradients and permanent off-resonance effects (i.e., for a fixed location in the voxel), and under the assumption of instantaneous RF pulses, the Bloch equations yield the following recurrence for the magnetization states just after RF pulses:

$$\mathbf{M}_{n+1}^+(\theta) = \mathbf{A}(\theta + \phi_n)\mathbf{M}_n^+(\theta) + \mathbf{B} \qquad [2]$$

where

$$\mathbf{A}(\theta) = \mathbf{R}_{x,\alpha}\mathbf{E}(TR)\mathbf{P}(\theta)$$

$$\mathbf{B} = (1 - E_1(TR))M_0\mathbf{R}_{x,\alpha}\mathbf{1}_z.$$

$\mathbf{R}_{x,\alpha}$ is the matrix describing a rotation of angle α around the x axis, $\mathbf{P}(\theta)$ a precession of θ around the $\mathbf{z}$ axis, $\mathbf{E}(t) = \text{diag}(E_2(t),\ E_2(t),\ E_1(t))$, $E_1(t) = \exp(-t/T_1)$, $E_2(t) = \exp(-t/T_2)$, M_0 is the thermal equilibrium magnetization, and $\mathbf{1}_z$ is the unit vector in the z direction. The simplified notations $E_1 = E_1(TR)$ and $E_2 = E_2(TR)$ will also be used in the following developments. Starting from some initial magnetization $\mathbf{M}_1^+$, the recursive application of Eq. [2] yields

$$\mathbf{M}_2^+(\theta) = \mathbf{A}(\theta + \phi_1)\mathbf{M}_1^+ + \mathbf{B}$$

$$\mathbf{M}_3^+(\theta) = \mathbf{A}(\theta + \phi_2)\mathbf{A}(\theta + \phi_1)\mathbf{M}_1^+ + \mathbf{A}(\theta + \phi_2)\mathbf{B} + \mathbf{B}$$

$$\mathbf{M}_4^+(\theta) = \mathbf{A}(\theta + \phi_3)\mathbf{A}(\theta + \phi_2)\mathbf{A}(\theta + \phi_1)\mathbf{M}_1^+ + \mathbf{A}(\theta + \phi_3)\mathbf{A}(\theta + \phi_2)\mathbf{B} + \mathbf{A}(\theta + \phi_3)\mathbf{B} + \mathbf{B}.$$

The linear evolution of ϕ_n (see Eq. [1]) allows us to write the general expression

$$\mathbf{M}_n^+(\theta - \phi_{n-1}) = \mathbf{A}(\theta)\mathbf{A}(\theta - \psi)\mathbf{A}(\theta - 2\psi)\dots\mathbf{A}(\theta - (n-2)\psi)\mathbf{M}_1^+ + [\mathbf{I} + \mathbf{A}(\theta) + \mathbf{A}(\theta)\mathbf{A}(\theta - \psi) + \mathbf{A}(\theta)\mathbf{A}(\theta - \psi)\mathbf{A}(\theta$$

$$- 2\psi) + \dots + \mathbf{A}(\theta)\mathbf{A}(\theta - \psi)\mathbf{A}(\theta - 2\psi)\dots\mathbf{A}(\theta - (n-3)\psi)]\mathbf{B}. \qquad [3]$$

where $\mathbf{I}$ is the unit 3×3 matrix. Since $E_2 \leq E_1$ it holds that

$$\forall\ \theta,\ \mathbf{M} : \|\mathbf{A}(\theta)\mathbf{A}(\theta - \psi)\mathbf{A}(\theta - 2\psi)\dots\mathbf{A}(\theta - n\psi)\mathbf{M}\|$$

$$\leq E_1^{n+1}\|\mathbf{M}\|,$$

hence, the first term in the right-hand side of Eq. [3] converges uniformly to zero for $n \to \infty$ because $E_1 < 1$. Also, since

$$\sum_{n=0}^{\infty} E_1^n = \frac{1}{1 - E_1},$$

the Weierstrass uniform convergence criterium for series (comparison criterium) (22) implies that

$$\lim_{n\to\infty} \mathbf{M}_n^+(\theta - \phi_{n-1}) = \mathbf{M}_{\text{pss}}(\theta) \qquad [4]$$

with

$$\mathbf{M}_{\text{pss}}(\theta) = [\mathbf{I} + \mathbf{A}(\theta) + \mathbf{A}(\theta)\mathbf{A}(\theta - \psi) + \mathbf{A}(\theta)\mathbf{A}(\theta - \psi)\mathbf{A}(\theta - 2\psi) + \dots]\mathbf{B} \qquad [5]$$

where the series at the right-hand side converges uniformly with respect to $\theta \in [0, 2\pi]$. Equation [4] demonstrates the remarkable property that, although the magnetization vector does not reach a steady state for each θ value separately (basically because the sequence is not periodic), at large n the magnetization profile $\mathbf{M}_n^+(\theta)$ becomes independent of n apart from a variable shift ϕ_{n-1}. Note that this limit, termed "pseudo-steady state" in the remainder of this article, is independent of the initial magnetization state $\mathbf{M}_1^+$. It is easily verified from Eq. [5] that the function $\mathbf{M}_{\text{pss}}(\theta)$ satisfies

$$\mathbf{M}_{\text{pss}}(\theta) = \mathbf{A}(\theta)\mathbf{M}_{\text{pss}}(\theta - \psi) + \mathbf{B}, \qquad [6]$$

which is also found by searching a solution of Eq. [2] of the form

$$\mathbf{M}_n^+(\theta) = \mathbf{M}_{\text{pss}}(\theta + \phi_{n-1}). \qquad [7]$$

or by replacing θ by $\theta - \phi_n$ in Eq. [2] and passing to the limit for $n \to \infty$. Interestingly, the uniform convergence of the sequence $\mathbf{M}_n^+(\theta - \phi_{n-1})$ (see Eq. [4]), the equation (Eq. [6]) defining the limit of this sequence, and the solution (Eq. [5]) of this equation, can be derived easily from general results of functional analysis, as shown in Appendix B.

If $\psi = 0$ (no RF spoiling), Eqs. [4], [5], and [6] reduce to the well-known result (23,24)

$$\lim_{n\to\infty} \mathbf{M}_n^+(\theta) = [\mathbf{I} - \mathbf{A}(\theta)]^{-1}\mathbf{B}. \qquad [8]$$

More generally, if $\phi = (K/P)(2\pi)$, with K and P integer, it holds that

$$\mathbf{M}_{\mathrm{pss}}(\theta) = [\mathbf{I} - \mathbf{A}(\theta)\mathbf{A}(\theta - \psi)\dots\mathbf{A}(\theta - (P-1)\psi)]^{-1}$$
$$\times [\mathbf{I} + \mathbf{A}(\theta) + \mathbf{A}(\theta)\mathbf{A}(\theta - \psi) + \dots$$
$$+ \mathbf{A}(\theta)\mathbf{A}(\theta - \psi)\dots\mathbf{A}(\theta - (P-2)\psi)]\mathbf{B}. \quad [9]$$

This result can be obtained either through a direct factorization of Eq. [5] or by substituting $\mathbf{M}_{\mathrm{pss}}(\theta - \psi) = \mathbf{A}(\theta - \psi)\mathbf{M}_{\mathrm{pss}}(\theta - 2\psi) + \mathbf{B}$ in the right-hand side of Eq. [6], substituting $\mathbf{M}_{\mathrm{pss}}(\theta - 2\psi) = \mathbf{A}(\theta - 2\psi)\mathbf{M}_{\mathrm{pss}}(\theta - 3\psi) + \mathbf{B}$ in the resulting equation, and so forth, and using the relation $\mathbf{A}(\theta - P\psi) = \mathbf{A}(\theta)$. In this case the sequence is actually periodical, with a period of $P \cdot TR$; hence, the same result can be obtained by expressing the condition that the magnetization vector found after the n-th RF pulse is equal to the magnetization found after the $(n + P)$-th pulse (see Refs. (25–27) for similar calculations). Although Eq. [9] provides an analytical expression of $\mathbf{M}_{\mathrm{pss}}(\theta)$ for specific values of ψ, it should be noted that the number of operations required to evaluate this formula grows rapidly with the periodicity P, leading to increasingly complex results. If $\psi/(2\pi)$ is irrational, that is, cannot be written as the ratio of two integer numbers, the sequence is not periodical and the properties used to obtain Eq. [9] are not applicable. Therefore, the task of finding an analytical expression of $\mathbf{M}_{\mathrm{pss}}(\theta)$ for an arbitrary value of ψ appears to be quite difficult, and might even be impossible. Of course, any irrational number can be seen as the limit of a sequence of rational numbers K/P with increasing P, but for $P \to \infty$ Eq. [9] leads back to the series expansion (Eq. [5]).

Existence of a Steady-State Signal Intensity: Integration Method

Until now we have studied the evolution of an isolated isochromat, that is, we have considered a fixed θ value. This is sufficient to describe signal formation in sequences with fully-balanced gradients per repetition interval (usually called TrueFISP, balanced-FFE, FIESTA, or balanced SSFP), since the good field homogeneity and short repetition times available nowadays on clinical scanners make it reasonable to consider that all spins in a voxel experience the same precession angle per TR. However, in RF-spoiled sequences, the varying precession angle ϕ_n prevents the magnetization vector from reaching a steady state for each isochromat separately (see Eqs. [4] and [7]); hence, the combination of RF spoiling with fully refocused gradients would generate strong signal variations from repetition to repetition, leading to image artifacts. Therefore, as stated above, the net gradient area per repetition interval needs to be large enough to ensure that the signal from a voxel results from the superposition of a wide range of θ values. Under this condition, and provided that the detector phase is set to $k\phi_{n-1}$ (see sequence description above), the signal collected after the n-th pulse is given by the following integral over precession angles:

$$S_{k,n} = e^{-ik\phi_{n-1}} \int\int E_2(TE)e^{i(-k\theta_{\mathrm{g}}+\delta\omega TE)}M_{\mathrm{T},n}^+(\theta_{\mathrm{g}}$$
$$+ \delta\omega TR)h(\theta_{\mathrm{g}}, \delta\omega)\, d\theta_{\mathrm{g}}d\delta\omega \quad [10]$$

where the complex notation $M_{\mathrm{T}} = M_x + iM_y$ is used for transverse magnetization and $h(\theta_{\mathrm{g}}, \delta\omega)$ is the joint distribution function of θ_{g} and $\delta\omega$ within a voxel. The factor $E_2(TE)\exp(i(-k\theta_{\mathrm{g}} + \delta\omega TE))$ describes the relaxation and precession occurring between excitation and readout. Under the assumption that θ_{g} and $\delta\omega$ are independent, θ_{g} being uniformly distributed between 0 and 2π, and $\delta\omega$ following a lorentzian distribution (mean $\delta\omega_0$, full width at half maximum $2/T_2'$) (13), the change of variable $\theta = \theta_{\mathrm{g}} + \delta\omega TR$ leads to

$$S_{k,n} = E_2(TE)e^{i(TE+kTR)\delta\omega_0-|TE+kTR|/T_2'}e^{-ik\phi_{n-1}}\langle e^{-ik\theta}M_{\mathrm{T},n}^+(\theta)\rangle, \quad [11]$$

where

$$\langle f(\theta)\rangle = \frac{1}{2\pi}\int_0^{2\pi} f(\theta)\,d\theta.$$

By operating the change of variable $\theta' = \theta + \phi_{n-1}$, passing to the limit for $n \to \infty$, permuting limit and integral (this is allowed in the case of uniform convergence (22)), and using Eq. [4], one finally obtains

$$S_{k,\mathrm{ss}} = \lim_{n\to\infty} S_{k,n} = E_2(TE)e^{i(TE+kTR)\delta\omega_0-|TE+kTR|/T_2'}\langle e^{-ik\theta}M_{\mathrm{T,pss}}(\theta)\rangle. \quad [12]$$

This shows that, with a large uncompensated gradient area per TR and the detector phase set to $k\phi_{n-1}$, the collected signal converges to a steady state value given by the product of 3 factors, the second one accounting for permanent off-resonance effects over the effective echo time $kTR + TE$, and the third one being the k-th Fourier coefficient of $M_{\mathrm{T,pss}}(\theta)$. For FLASH imaging ($k = 0$) this means that, without detector phase modulation, the MR signal converges towards a constant value given by the product of the DC component of $\mathbf{M}_{\mathrm{pss}}(\theta)$ with a factor describing T_2^* decay ($T_2^{*-1} = T_2^{-1} + T_2'^{-1}$) and dephasing over the time to echo TE. Note that, due to the equivalence demonstrated in Appendix A, the same result holds for FLASH sequences with quadratic pulse phase variation, provided that the detector phase is equal to the phase of the last RF pulse.

On the basis of Eqs. [12] and [5], it is possible to derive (see proof in Appendix C) the property that, if $\delta\omega_0 = 0$,

$$S_{k,\mathrm{ss}}(-\psi) = -S_{k,\mathrm{ss}}^\star(\psi). \quad [13]$$

This result means that signal in the y channel is a symmetric function of ψ, while the x component is antisymmetric. As a consequence, the analysis of RF spoiled gradient-echo sequences can be restricted to ψ values in the interval $[0, \pi]$, and at $\psi = 0$ the x component of $S_{k,\mathrm{ss}}$ is zero for any value of k.

Since no general analytical expression has been found for $\mathbf{M}_{\mathrm{pss}}(\theta)$, the integral in Eq. [12] cannot be calculated explicitly for arbitrary ψ values. If $\psi = (K/P)(2\pi)$, with K and P integer, the signal intensity can in principle be obtained by integrating Eq. [9], for example, using symbolic calculus software, but the resulting expressions are

very cumbersome even for moderate values of K and P. Note that the lack of analytical expression for the steady-state signal intensity for irrational values of $\psi/2\pi$ is more a formal than a practical problem, since any digital phase generator will be based on a finite number of control bits, so the phase step will be a rational number.

Physical Decomposition of the Steady-State Signal: Partition Method

In the previous section, the integration method has been used to prove that a steady-state signal intensity is reached with RF-spoiled sequences if the uncompensated gradient area is large enough to induce a uniform distribution of precession angles within each voxel and if the detector phase is properly modulated. However, this approach has provided little intuition about the basic mechanisms of signal formation. Here, the partition method introduced initially by Kaiser and co-workers (11) and further justified in Ref. (13) for the coherent case, is extended to the case of linearly varying precession angles, in order to interpret the steady-state signal as a sum of gradient, spin, and stimulated echoes. The ultimate goal is to quantify the different coherence pathways involved in signal formation, in order to assess their degree of interference as functions of the phase increment ψ. The analysis is restricted to FLASH, PSIF, and ES-FFE sequences, and the effect of permanent off-resonance effects is not considered, since this problem is efficiently treated by means of the integration method (see above).

As shown in Appendix D, when the pseudo-steady state is established, that is, $n \to \infty$ (this will be tacitly assumed in the remainder of this section), the transverse magnetization after the n-th pulse can be written as

$$M_{T,n}^+(\theta) = M_{x,n}^+(\theta) + iM_{y,n}^+(\theta) = \sum_{\ell=1}^{\infty} \sum_{\{q_1\ldots q_\ell\}|q_\ell=\pm 1} \mu_{n,\{q_1\ldots q_\ell\}}(\theta).$$

[14]

In this expression, each term $\mu_{n,\{q_1\ldots q_\ell\}}(\theta)$ can be viewed as a part of $M_{T,n}^+(\theta)$ that finds its origin in the homogeneous magnetization generated earlier by pulse number $n - \ell + 1$, and has evolved during $(\ell - 1)$ repetition intervals under the effect of precession, relaxation, and rotations due to RF pulses. The indices q_j indicate whether the magnetization component was longitudinal ($q_j = 0$) or transverse ($q_j = \pm 1$) during a particular repetition interval, with a distinction between defocusing ($q_j = 1$) and refocusing ($q_j = -1$) components. The sequence $\{q_1 \ldots q_{\ell-1}\}$ remembers thus the history of the component from pulse $(n - \ell + 1)$ to pulse n and q_ℓ gives the status of the component during the n-th *TR* interval, that is, between pulses n and $n + 1$. The first term $\mu_{n,1}(\theta)$ is the homogeneous part (or DC component) of the pseudo-steady state transverse magnetization, that is, $\langle M_{T,pss}(\theta)\rangle$. This quantity is equal to the homogeneous transverse magnetization just after any RF pulse in the pseudo-steady state (see Eq. [7]) and will be noted $\langle M_T^+\rangle$ in the following equations. The higher order components ($\ell > 1$) are obtained from this initial component by the iterative application of Eqs. [44] to [49] (see Appendix D). Each pulse

splits any existing magnetization component into 1 longitudinal component, 1 transverse dephasing component, and 1 transverse refocusing component. This process can be represented by a tree where each node gives rise to 3 branches (11,13). The tree of magnetization paths is stopped when the dephasing index $\sigma_\ell = \Sigma_{k=1}^{\ell} q_k$ vanishes, that is, at nodes that would give rise to fully refocused components at the next level in the tree. This is a consequence of the second term of Eq. [43] and can be interpreted as the fact that all components originating from these nodes are already taken into account, since the root of the partition tree is the homogeneous transverse magnetization just after the RF pulse.

For a FID measurement (T1-FFE or FLASH, $k = 0$), no dephasing occurs between excitation and readout; hence, the signal is proportional to the single homogeneous term in Eq. [14], which is the root of the partition tree:

$$S_{\text{FLASH}} = E_2(TE)\mu_{n,1}(\theta) = E_2(TE)\langle M_T^+\rangle.$$

[15]

Note that $\langle M_T^+\rangle$ might be evaluated numerically by means of the Fourier expansion method (see below) but is not determined by the partition method at this stage.

In PSIF sequences (or CE-FAST or T2-FFE, $k = -1$), the magnetization precesses by θ between excitation and readout; thus, only the terms proportional to $e^{-i\theta}$ in Eq. [14] (i.e., those satisfying $\sigma_\ell = 0$) give rise to coherent contributions at the time of data sampling. The signal intensity is therefore given by

$$S_{\text{PSIF}} = E_2(TE)e^{i(\theta+\phi_{n-1})} \sum_{\ell=1}^{\infty} \sum_{\sigma_\ell=0} \mu_{n,\{q_1\ldots q_\ell\}}(\theta)$$

[16]

where the factor $e^{i\phi_{n-1}}$ accounts for the detector phase modulation, and the dependence in θ vanishes because of the product of $e^{i\theta}$ with factors proportional to $e^{-i\theta}$ in the selected components $\mu_{n,\{q_1\ldots q_\ell\}}(\theta)$. Since the net gradient area between the readout and the next RF pulse is zero, the pathways selected in a PSIF experiment are the same as those contributing to the homogeneous magnetization just before the RF pulse, which is thus proportional to the PSIF signal:

$$\langle M_T^-\rangle = E_2 e^{i(\theta+\phi_n)} \sum_{\ell=1}^{\infty} \sum_{\sigma_\ell=0} \mu_{n,\{q_1\ldots q_\ell\}}(\theta) = e^{i\psi} E_2(TR - TE)S_{\text{PSIF}}.$$

[17]

As a consequence, the PSIF acquisition scheme is of little interest for practical applications since the goal of RF spoiling is to reduce as much as possible the residual transverse magnetization at the end of the repetition interval. However, the knowledge of $\langle M_T^-\rangle$ is informative from the point of view of sequence design since it reflects the efficiency of RF spoiling and, as shown below, can be used to evaluate the root of the partition tree $\langle M_T^+\rangle$. Table 1 lists the pathways satisfying $\sigma_\ell = 0$ (termed refocused pathways) of length $\ell \leq 5$, and the corresponding contributions to the homogeneous magnetization before the $(n + 1)$-th pulse. Note that all of them are independent of n, due to

Table 1
Refocused Pathways ($\sigma_\ell = \Sigma_{j=1}^{\ell} q_j = 0$) of Length $\ell \leq 5$ and Corresponding Contributions to the Homogeneous Magnetization Just Before the $(n + 1)$-th Pulse

Pathway:	Contribution to coherent magnetization before $(n + 1)$-th pulse:
$\{q_1 \ldots q_\ell\}$	$E_2 e^{i(\theta + \phi_n)} \mu_{n,\{q_1 \ldots q_\ell\}}(\theta)$
{1-1}	$\sin^2(\alpha/2) E_2^2 e^{i(\phi_n - \phi_{n-1})} \langle M_T^+ \rangle^*$
{10-1}	$\frac{1}{2} \sin^2\alpha E_1 E_2^2 e^{i(\phi_n - \phi_{n-2})} \langle M_T^+ \rangle^*$
{11-1-1}	$\cos^4(\alpha/2)\sin^2(\alpha/2) E_2^4 e^{i(\phi_n + \phi_{n-1} - \phi_{n-2} - \phi_{n-3})} \langle M_T^+ \rangle^*$
{100-1}	$\frac{1}{2} \cos\alpha \, \sin^2\alpha E_1^2 E_2^2 e^{i(\phi_n - \phi_{n-3})} \langle M_T^+ \rangle^*$
{110-1-1}	$\frac{1}{2} \sin^2\alpha \, \cos^4(\alpha/2) E_1 E_2^4 e^{i(\phi_n + \phi_{n-1} - \phi_{n-3} - \phi_{n-4})} \langle M_T^+ \rangle^*$
{11-10-1}	$-\frac{1}{2} \sin^2\alpha \, \cos^2(\alpha/2)\sin^2(\alpha/2) E_1 E_2^4$ $\times \, e^{i(\phi_n + \phi_{n-2} - \phi_{n-3} - \phi_{n-4})} \langle M_T^+ \rangle^*$
{101-1-1}	$-\frac{1}{2} \sin^2\alpha$ $\sin^2(\alpha/2)\cos^2(\alpha/2) E_1 E_2^4 e^{i(\phi_n + \phi_{n-1} - \phi_{n-2} - \phi_{n-4})}$ $\times \, \langle M_T^+ \rangle^*$
{1000-1}	$\frac{1}{2} \cos^2\alpha \, \sin^2\alpha E_1^3 E_2^2 e^{i(\phi_n - \phi_{n-4})} \langle M_T^+ \rangle^*$

Pathways associated with second order terms in α are emphasized in bold. All components are proportional to $\langle M_T^+ \rangle^*$. They are also independent of n, since ϕ_n is a linear function of n and the number of positive phase terms equals the number of negative terms. PSIF signal components during the n-th repetition interval can be obtained by multiplying with $E_2(TE - TR)e^{-i\psi}$.

the linear variation of ϕ_n and the fact that $\sigma_\ell = 0$ is possible only if the number of refocusing periods along the pathway equals the number of defocusing periods. This means that the PSIF signal and the homogeneous magnetization just before the RF pulse are stationary in the pseudo-steady state, in agreement with the results of the integration method, with Eq. [7], and with the relationship between magnetization vectors before and after a RF pulse: $\mathbf{M}_n^+(\theta) = \mathbf{R}_{x,\alpha} \mathbf{M}_n^-(\theta)$. Table 1 illustrates also the property that all terms in Eq. [17] are proportional to $\langle M_T^+ \rangle^*$; hence, Eq. [17] is actually a proportionality relationship between $\langle M_T^- \rangle$ and $\langle M_T^+ \rangle^*$, the factor

$$C = \frac{\langle M_T^- \rangle}{\langle M_T^+ \rangle^*} = E_2 e^{i\psi} \frac{S_{\text{PSIF}}}{S_{\text{FLASH}}^*} \qquad [18]$$

being given by a series expansion, where each term is the product of a real factor related to relaxation and RF pulses, times a phase factor due to RF spoiling. As a consequence, C is purely real in the coherent case ($\psi = 0$).

In the small flip angle limit, the summation over refocused pathways appearing in the expressions of S_{PSIF} (Eq. [16]) and $\langle M_T^- \rangle$ (Eq. [17]) can be further restricted to the second order expansion in α, that is, to pathways of the form $\{(1)_p(0)_j(-1)_p\}$ ($p \geq 1, j \geq 0$). Indeed, each direct transition from $q_\ell = \pm 1$ to $q_{\ell+1} = \mp 1$ introduces a factor $\sin^2(\alpha/2)$ (see Eq. [46]), and any indirect transition from $q_{\ell-j} = \pm 1$ to $q_{\ell+1} = \mp 1$ with storage as longitudinal magnetization in the mean time gives rise to a factor $(\sin^2\alpha)/2$ (see Eqs. [45] and [49]). Using the linear evolution of ϕ_n, it follows that C can be approximated as follows:

$$C \approx E_2^2 \frac{\alpha^2}{2} \left(\frac{e^{i\psi}}{2} + E_1 e^{i2\psi} + E_1^2 e^{i3\psi} + E_1^3 e^{i4\psi} + \ldots \right)$$

$$+ E_2^4 \frac{\alpha^2}{2} \left(\frac{e^{i4\psi}}{2} + E_1 e^{i6\psi} + E_1^2 e^{i8\psi} + E_1^3 e^{i10\psi} + \ldots \right)$$

$$+ E_2^6 \frac{\alpha^2}{2} \left(\frac{e^{i9\psi}}{2} + E_1 e^{i12\psi} + E_1^2 e^{i15\psi} + E_1^3 e^{i18\psi} + \ldots \right) + \ldots$$

where the first row is the sum of all pathways of the form $\{1(0)_j - 1\}$ ($p = 1, j = 0, 1, 2, 3 \ldots$), the second row corresponds to pathways of the type $\{11(0)_j - 1 - 1\}$ ($p = 2, j = 0, 1, 2, 3 \ldots$), and so forth. By defining the function

$$H(\psi) = \frac{1}{2} + \sum_{j=1}^{\infty} (E_1 e^{ij\psi})^j = \frac{1}{2} \frac{(1 - E_1^2) + 2i \sin\psi}{1 - 2E_1\cos\psi + E_1^2} \qquad [19]$$

the small flip angle approximation of C can be rewritten as

$$C \approx \frac{\alpha^2}{2} \sum_{p=1}^{\infty} E_2^{2p} e^{ip^2\psi} H(p\psi). \qquad [20]$$
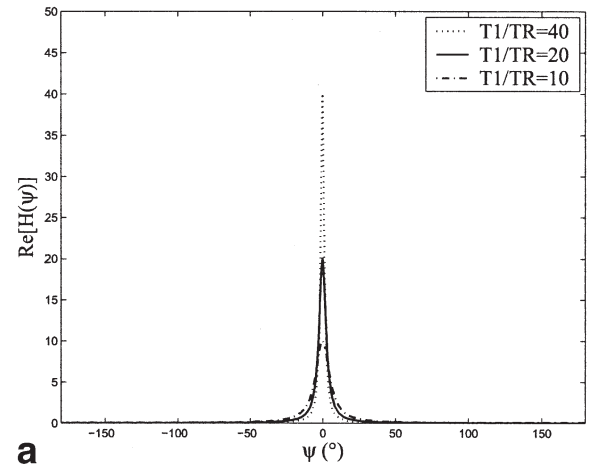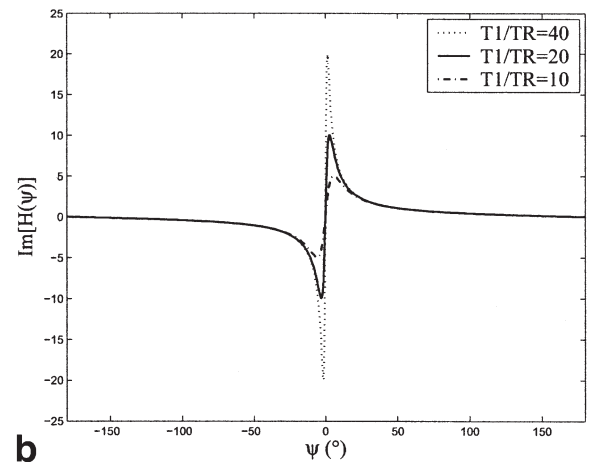
FIG. 2. Real (absorption) and imaginary (dispersion) parts of the function $H(\psi) = (1 - \exp(i\psi - TR/T_1))^{-1} - 1/2$ for $T_1/TR = 10, 20,$ and 40.

As shown by Fig. 2, the shape of $H(\psi)$ is that of a peak centered at $\psi = 0$, with an absorption (real) and a dispersion (imaginary) part. For large values of T_1/TR, the peak height of the real part can be approximated by T_1/TR and its full width at half maximum by $\sqrt{2} \cdot TR/T_1$. Note that these characteristics can be explained easily on the basis of the power series expansion in Eq. [19]: the value of H at $\psi = 0$ results from the coherent addition of numerous components with equal phases, giving rise to a maximum intensity, while at $\psi \neq 0$ each term has a different phase, leading to a reduced sum. If $E_1 \approx 1$ (i.e., $TR/T_1 \ll 1$) and ψ is not close to 0, numerous terms with approximately the same intensity interfere destructively due to their phase difference, while small E_1 or ψ values cause the component intensity to decrease significantly before a sufficient phase spread has been achieved, leading to incomplete cancellation. Knowing the shape of $H(\psi)$, it is possible to predict the structure of the graph of C versus ψ in the small flip angle limit, using Eq. [20]. The first term, which is due to the sum of refocused pathways of the form $\{1(0)_j - 1\}$ ($j = 0, 1, 2, 3 \ldots$), is proportional to $H(\psi)$; hence, it gives rise to peaks at $\psi = 0$ and $\psi = 2\pi$, as illustrated by Fig. 3a ($T_1/TR = 20$, $T_2 = T_1$, $\alpha = 10°$). The second term, related to pathways $\{11(0)_j - 1 - 1\}$ ($j = 0, 1, 2, 3 \ldots$), is proportional to $H(2\psi)$, leading to additional contributions to the peaks at $\psi = 0$ and 2π, as well as a new peak at $\psi = \pi$ (Fig. 3b). The contributions from the second term are smaller than those due to the first term, because of the factor E_2^{2P}. Adding the third term ($p = 3$) contributes to the peaks at $\psi = 0$ and 2π and introduces new peaks at $\psi = \frac{1}{3}(2\pi)$ and $\frac{2}{3}(2\pi)$ (Fig. 3c). The fourth term contributes to the peaks at $\psi = 0$, π, and 2π, and introduces new peaks at $\psi = \frac{1}{4}(2\pi)$ and $\psi = \frac{3}{4}(2\pi)$ (Fig. 3d). As a general rule, the p-th term, due to refocused pathways of the form $\{(1)_p(0)_j(-1)_p\}$ ($j = 0, 1, 2, 3 \ldots$), consists of p equidistant scaled replications of $H(\psi)$ in the $[0, 2\pi]$ interval. Consequently, it involves contributions at $\psi = (1/p)(2\pi)$, $(2/p)(2\pi), \ldots, 2\pi$, leading to new peaks for irreducible fractions of 2π and adding to existing peaks otherwise. The positions along the ψ axis of all peaks generated by the first p terms are therefore given by the set of irreducible fractions K/P satisfying $0 \leq K \leq P \leq p$, which is known as the p-th Farey sequence $\mathscr{F}_p$ (28):

$$\mathscr{F}_1 = \left\{ \frac{0}{1}, \frac{1}{1} \right\}$$

$$\mathscr{F}_2 = \left\{ \frac{0}{1}, \frac{1}{2}, \frac{1}{1} \right\}$$

$$\mathscr{F}_3 = \left\{ \frac{0}{1}, \frac{1}{3}, \frac{1}{2}, \frac{2}{3}, \frac{1}{1} \right\}$$

$$\mathscr{F}_4 = \left\{ \frac{0}{1}, \frac{1}{4}, \frac{1}{3}, \frac{1}{2}, \frac{2}{3}, \frac{3}{4}, \frac{1}{1} \right\}$$

$$\mathscr{F}_5 = \left\{ \frac{0}{1}, \frac{1}{5}, \frac{1}{4}, \frac{1}{3}, \frac{2}{5}, \frac{1}{2}, \frac{3}{5}, \frac{2}{3}, \frac{3}{4}, \frac{4}{5}, \frac{1}{1} \right\}$$

$$\vdots$$
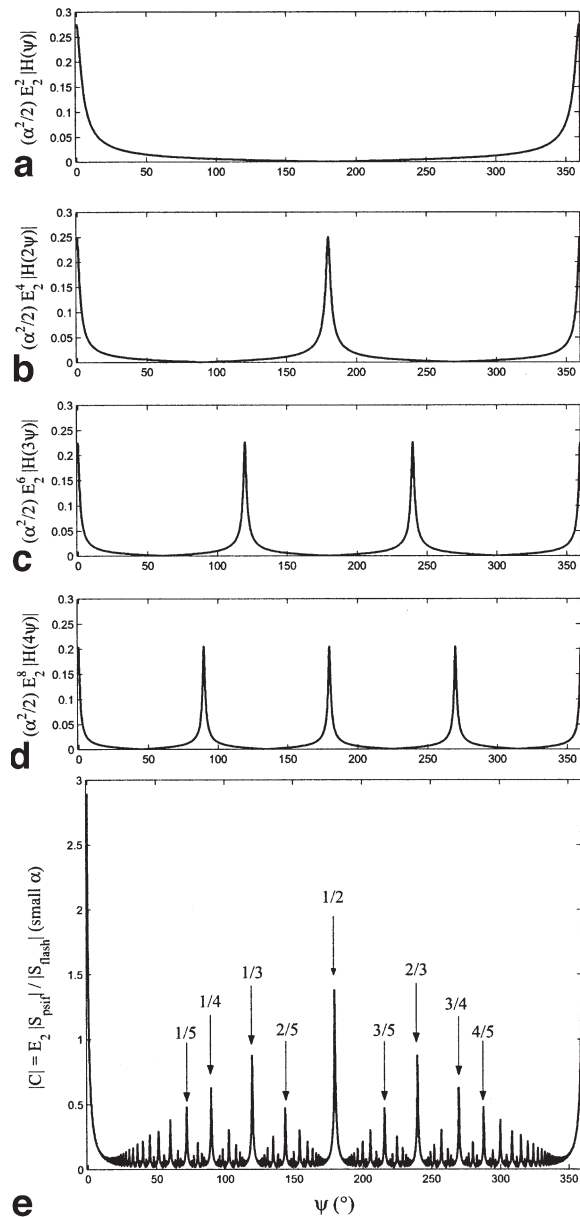
FIG. 3. (**e**) Small flip angle approximation of $|C|$, that is, E_2 times the ratio between PSIF and FLASH signal magnitudes, or equivalently the ratio between absolute values of the coherent transverse magnetization at the end and the beginning of the repetition interval. Parameter values are $\alpha = 10°$, $T_1/TR = 20$, $T_2 = T_1$, and ψ variable. The values were obtained by truncating the sum in Eq. [20] to 500 terms. (**a**)–(**d**) Contributions of terms $p = 1$ to $p = 4$, that is, of refocused pathways of the form $\{(1)_p(0)_j(-1)_p\}$ with $p = 1$ to 4. All irreducible fractions K/P with the same P value give rise to peaks with a similar height, which is a decreasing function of P.

Interestingly, $\mathscr{F}_{p+1}$ can be obtained from $\mathscr{F}_p$ by inserting the mediant fraction $(a + c)/(b + d)$ between the fractions a/b and c/d in the original set if $b + d \leq p + 1$ (28). When all terms in Eq. [20] are taken into account (see Fig. 3e), peaks are found at all ψ values of the form $(K/P)(2\pi)$, with K and P integer. If K/P is irreducible, the dominant contributions to the peak are due to terms $p = P$, $p = 2P$, $p =$

3P, and so forth. Assuming negligible contributions from the tails of other peaks, the values of C at $\psi = (K/P)(2\pi)$ is given by

$$\frac{\alpha^2}{2} \sum_{j=1}^{\infty} E_2^{2jP} H(0)$$

which is real, independent of K, and decreasing with P. For the parameter values of Fig. 3, the assumption of non-overlapping peaks is acceptable, for example, at $\psi = \frac{1}{5}(2\pi)$, $\frac{2}{5}(2\pi)$, $\frac{3}{5}(2\pi)$, and $\frac{4}{5}(2\pi)$, since these peaks have approximately the same amplitude, but does not hold in the vicinity of large peaks, near $\psi = 0$, for example. Note also that the graph of C versus ψ (Fig. 3e) is symmetric about $\psi = 180°$, in accordance with Eq. [13]. In summary, in the small flip angle limit, we have demonstrated that a deviation from $C = 0$, that is, imperfect spoiling of the coherent transverse magnetization just before RF pulses, occurs at all ψ values of the form $(K/P)(2\pi)$, with K and P integer. Assuming that K/P is irreducible, this deviation originates from the incomplete destructive interference between pathways of the form $\{(1)_P (0)_j (-1)_P\}$, $\{(1)_{2P} (0)_j (-1)_{2P}\}$, $\{(1)_{3P} (0)_j (-1)_{3P}\}$, ... Since T_2 relaxation attenuates transverse components (corresponding to $+1$ and -1 indices) the amplitude of the deviation decreases with P.

As proposed initially by Kaiser and colleagues (11) in the coherent case, the knowledge of the ratio $\langle M_T^- \rangle / \langle M_T^{+*} \rangle$ (or, equivalently, the knowledge of S_{PSIF}/S_{FLASH}^*) can be used to evaluate $\langle M_T^+ \rangle$, that is, to find the initial condition needed to completely determine the magnetization components in the partition tree. This is achieved by expressing the effect of a RF pulse on homogeneous magnetization components:

$$\langle M_T^+ \rangle = \cos^2 \frac{\alpha}{2} \langle M_T^- \rangle + \sin^2 \frac{\alpha}{2} \langle M_T^- \rangle^* - i \sin \alpha \langle M_z^- \rangle \quad [21]$$

$$\langle M_z^+ \rangle = \frac{\sin \alpha}{2i} (\langle M_T^- \rangle - \langle M_T^- \rangle^*) + \cos \alpha \langle M_z^- \rangle \quad [22]$$

and the effect of T_1 relaxation on the homogeneous longitudinal magnetization:

$$\langle M_z^- \rangle = E_1 \langle M_z^+ \rangle + (1 - E_1) M_0. \quad [23]$$

By solving the set of Eqs. [18], [21], [22], and [23], one finds $\langle M_T^+ \rangle$:

$$\langle M_y^+ \rangle = Im(\langle M_T^+ \rangle)$$

$$= \frac{-\sin \alpha (1 - E_1) M_0}{(1 - E_1 \cos \alpha) + (\cos \alpha - E_1)\left(Re(C) - \dfrac{[Im(C)]^2}{1 - Re(C)}\right)} \quad [24]$$

$$\langle M_x^+ \rangle = Re(\langle M_T^+ \rangle) = \frac{Im(C)}{1 - Re(C)} \langle M_y^+ \rangle \quad [25]$$

where Re and Im denote the real and imaginary parts of a complex number, respectively. Equations [24] and [25] generalize the expressions found in Ref. (11) (Eqs. [46] and [47]) for coherent sequences ($\psi = 0$, no RF spoiling). In that case, $Im(C) = 0$ (see above) and $Re(\langle M_T^+ \rangle) = 0$ (see Eq. [25]), in accordance with the symmetry result obtained above (Eq. [13]). In the limiting case of $C = 0$ (i.e., $\langle M_T^- \rangle = 0$, $S_{PSIF} = 0$), termed ideal spoiling, the FLASH signal reduces to the Ernst formula (1–3) found at $TR \gg T_2$. As a consequence of the previous discussion, in the small flip angle limit, the largest deviations from ideal spoiling occur at ψ values of the form $(K/P)(2\pi)$. At these ψ values, $Re(C)$ is large and $Im(C)$ is close to zero; hence, the FLASH signal is essentially imaginary and the sign of the deviation from ideal spoiling is conditioned by the factor $(\cos \alpha - E_1)$ appearing in the denominator of Eq. [24]. Flip angle values below the Ernst angle ($\alpha < \alpha_E = \arccos(E_1)$) yield negative deviations, $\alpha > \alpha_E$ gives rise to local maxima for the signal intensity, and at $\alpha = \alpha_E = \arccos(E_1)$ (Ernst angle) the y component of the FLASH signal is equal to the ideal spoiling signal, independently of the value of ψ. These theoretical predictions are in agreement with the observations made with numerical simulations and experiments (4–6,8).

In echo-shifted sequences, the pathways leading to coherent magnetization at the time of echo are those proportional to $e^{i\theta}$ (termed ES pathways). The signal intensity is obtained by selecting these terms in Eq. [14] and multiplying the result with $E_2(TE)e^{-i(\theta + \phi_{n-1})}$ to account for transverse relaxation, gradient-related precession during the delay between excitation and readout, and detector phase modulation:

$$S_{ES-FFE} = E_2(TE)e^{-i(\theta + \phi_{n-1})} \sum_{\ell=1}^{\infty} \sum_{\sigma_{\ell-1}=1, q_\ell=1} \mu_{n,\{q_1...q_\ell\}}(\theta). \quad [26]$$

Note that the dependence in θ vanishes because of the product of $e^{-i\theta}$ with the factor $e^{i\theta}$ appearing in all selected components. The contributions due to ES pathways with $\ell = 1$ to 5 are given in Table 2. Due to the linear evolution of ϕ_n and the equal number of negative and positive contributions to the RF spoiling-related phase, all contributions are independent of n; hence, the ES-FFE signal is stationary in the pseudo-steady state, in agreement with the results of the integration method. Note also that all terms contain the factor $\langle M_T^+ \rangle$; hence, Eq. [26] is a proportionality relationship between S_{ES-FFE} and $\langle M_T^+ \rangle$ (or equivalently S_{FLASH}). In the small flip angle approximation (second order expansion in α) only the primary ES pathway $\{11\}$ and the "dominant" secondary ES pathways $\{1(0)_j 1\}$ ($j = 1, 2, 3, ...$) (13) are retained in the summation since all other ES pathways involve at least 2 transitions from refocusing to defocusing transverse magnetization, or vice versa. The ratio of ES-FFE and FLASH signals can then be approximated as follows:

$$S_{ES-FFE}/S_{FLASH} \approx E_2$$

$$\times \left(\cos^2 \frac{\alpha}{2} - \frac{\alpha^2}{2} (E_1 e^{-i\psi} + E_1^2 e^{-2i\psi} + E_1^3 e^{-3i\psi} + ...)\right) \quad [27]$$

Table 2
Echo-Shifted Pathways ($\sigma_{\ell-1} = \sum_{j=1}^{\ell-1} q_j = 1$, $q_\ell = 1$) of Length $\ell \leq 5$ and Corresponding Contributions to the Steady-State Signal in Spoiled ES-FFE Sequences

Pathway: $\{q_1 \ldots q_\ell\}$	Contribution to ES-FFE signal after n-th pulse: $E_2(TE)e^{i(-\theta-\phi_{n-1})}\mu_{n_1}\{q_1 \ldots q_\ell\}(\theta)$
{11}	$\cos^2(\alpha/2)E_2(TR + TE)\langle M_T^+\rangle$
{101}	$-\frac{1}{2}\sin^2\alpha E_1 E_2(TR + TE)e^{i(-\phi_{n-1}+\phi_{n-2})}\langle M_T^+\rangle$
{11-11}	$\cos^2(\alpha/2)\sin^4(\alpha/2)E_2(3TR + TE)$ $\times e^{i(-\phi_{n-1}-\phi_{n-1}+\phi_{n-2}+\phi_{n-3})}\langle M_T^+\rangle$
{1001}	$-\frac{1}{2}\cos\alpha\,\sin^2\alpha E_1^2 E_2(TR + TE)e^{i(-\phi_{n-1}+\phi_{n-3})}\langle M_T^+\rangle$
{110-11}	$\frac{1}{2}\sin^2\alpha\,\cos^2(\alpha/2)\sin^2(\alpha/2)E_1 E_2(3TR + TE)$ $\times e^{i(-\phi_{n-1}-\phi_{n-1}+\phi_{n-3}+\phi_{n-4})}\langle M_T^+\rangle$
{11-101}	$\frac{1}{2}\sin^2\alpha\,\cos^2(\alpha/2)\sin^2(\alpha/2)E_1 E_2(3TR + TE)$ $\times e^{i(-\phi_{n-1}-\phi_{n-2}+\phi_{n-3}+\phi_{n-4})}\langle M_T^+\rangle$
{101-11}	$-\frac{1}{2}\sin^2\alpha\,\sin^4(\alpha/2)E_1 E_2(3TR + TE)$ $e^{i(-\phi_{n-1}-\phi_{n-1}+\phi_{n-2}+\phi_{n-4})}\langle M_T^+\rangle$
{10001}	$-\frac{1}{2}\cos^2\alpha\,\sin^2\alpha E_1^3 E_2(TR + TE)e^{i(-\phi_{n-1}+\phi_{n-4})}\langle M_T^+\rangle$

Pathways associated with second order terms in α are emphasized in bold. All components are proportional to $\langle M_T^+\rangle$. They are also independent of n, since ϕ_n is a linear function of n and the number of positive phase terms equals the number of negative terms.

$$\approx E_2\left(\left(1 - \frac{\alpha^2}{4}\right) - \frac{\alpha^2}{2}\left(H(-\psi) - \frac{1}{2}\right)\right). \qquad [28]$$

At $\psi = 0$ (coherent ES-FFE sequences) the term $(-\alpha^2/2)(H(0) - 1/2)$, which is due to the coherent addition of pathways of the type $\{1(0)_j1\}$ ($j = 1, 2, 3, \ldots$), tends to reduce the ratio $S_{\text{ES-FFE}}/S_{\text{FLASH}}$, leading to a net value smaller than $E_2\cos(\alpha^2/2)$, that is, the value that would be expected if only the primary ES pathway contributed (13). When RF spoiling is applied, $H(-\psi)$ decays rapidly with ψ because of the different phases acquired by secondary ES pathways. Therefore the destructive interference between primary and secondary ES pathways disappears and, far from $\psi = 0$, the ratio $S_{\text{ES-FFE}}/S_{\text{FLASH}}$ is even larger than $E_2\cos^2(\alpha/2)$.

NUMERICAL SIMULATIONS

In this section we assess the accuracy of the partition method in the small flip angle regime by comparing it with "exact" signal intensities. The calculation of these values is not trivial since no general analytical expressions have been obtained so far. In principle it would be possible to evaluate $\mathbf{M}_{\text{pss}}(\theta)$ for a large number of θ values by truncating the series expansion in Eq. [5], and to obtain the signal intensity by averaging over θ values (see Eq. [12]). However, the errors introduced by approximating the series and the integral with finite sums would not be easily assessed. Another approach would be to evaluate the series resulting from the partition method, without restricting the summation to second order terms. In practice, this approach is also not feasible since the number of components to be evaluated grows exponentially with the number of pulses applied, leading to prohibitive computing

times, especially when $TR \ll T_1$ (11). The solution that has been adopted most often (5–8) consists of evaluating the recurrence in Eq. [2] for a "large" number of θ values and averaging the resulting magnetization vectors to obtain the transient signal intensities as given by Eq. [11]. After a sufficient number of TR intervals, a good approximation of the steady-state signal is obtained. This approach is conceptually simple because it closely mimics the physical mechanism of signal formation, but in practice it can be time consuming since the magnetization vector evolution needs to be calculated many times and the minimum number of isochromats required to achieve a given precision is not easily determined. As shown in Refs. (9,14) and chapter 8 of Ref. (2), an elegant solution to these problems consists of translating the recurrence for $\mathbf{M}_n^+(\theta)$ into a recurrence for the Fourier coefficients of this function, which are directly proportional to signal intensities. Here this approach is adapted to the case of linearly varying precession angles, and an estimate of the minimum number of pulses required to reach steady-state with a given accuracy is provided. The method is then applied to RF-spoiled FLASH, PSIF, and ES-FFE, and the results are compared to those obtained by means of the partition method in the small flip angle approximation.

Computational Algorithm for Transient and Steady-State Signals: Fourier Expansion Method

Since $\mathbf{M}_n^+(\theta)$ is a periodic function of θ, its transverse and longitudinal parts can be written as two Fourier series

$$M_{T,n}^+(\theta) = \sum_k F_{k,n}M_0e^{ik\theta} \qquad [29]$$

$$M_{z,n}^+(\theta) = \sum_k G_{k,n}M_0e^{ik\theta} \qquad [30]$$

where $G_{-k,n} = G_{k,n}^*$ since $M_{z,n}^+(\theta)$ is real. By expressing Eq. [2] in the coordinate system (M_T, M_T^*, M_z), with $M_T = M_x + iM_y$ (2) one obtains the following recurrence for the Fourier coefficients:

$$F_{k,n+1} = E_2\cos^2\frac{\alpha}{2}e^{i\phi_n}F_{k-1,n} + E_2\sin^2\frac{\alpha}{2}e^{-i\phi_n}F_{-k-1,n}^*$$
$$- iE_1\sin\alpha G_{k,n} - i\sin\alpha(1 - E_1)\,\delta_{k,0} \quad [31]$$

$$G_{k,n+1} = -\frac{i}{2}E_2\sin\alpha e^{i\phi_n}F_{k-1,n} + \frac{i}{2}E_2\sin\alpha e^{-i\phi_n}F_{-k-1,n}^*$$
$$+ E_1\cos\alpha G_{k,n} + \cos\alpha(1 - E_1)\,\delta_{k,0} \quad [32]$$

where $\delta_{i,j} = 1$ when $i = j$ and 0 otherwise (Kronecker's delta). If the spin system is at equilibrium when the sequence is started, the magnetization state after the first RF pulse is given by $\mathbf{M}_1^+ = \mathbf{R}_{x,\alpha}M_0\mathbf{1}_z$, that is,

$$F_{k,1} = -i\sin\alpha\,\delta_{k,0} \qquad [33]$$

$$G_{k,1} = \cos\alpha\,\delta_{k,0}. \qquad [34]$$

Every new RF pulse in the train fills 2 additional coherence levels; hence, after the n-th pulse, non-zero coefficients are found for $-n - 1 \leq k \leq n - 1$.

According to Eq. [11] the signal measured during the n-th interpulse interval is directly proportional to the k-th Fourier coefficients of $M_{T,n}^+(\theta)$:

$$S_{k,n}/M_0 = E_2(TE)e^{i(TE+kTR)\delta\omega_0 - |TE+kTR|/T_2'}e^{-ik\phi_{n-1}}F_{k,n}$$

and an approximation of the steady-state signal intensity $S_{k,ss}$ can be obtained by the recursive application of Eqs. [31] and [32] until sufficient convergence has been reached. As shown in Appendix E, the minimum number of TR intervals required to achieve a precision of $\epsilon \cdot M_0$ is given by

$$n = -(\ln(\epsilon/2) + TE/T_2)T_1/TR + 1 \qquad [35]$$

independently of the initial magnetization state.

Results

Figure 4 shows the "exact" values of $|C|$, that is, the ratio of PSIF and FLASH modulus signals (see Eq. [18]), as functions of the phase increment ψ. These values have been obtained using the Fourier expansion method (Eqs. [31] and [32]) with the following parameters: $T_1/TR = 20$, $T_2 = T_1$, $\alpha = 10°$, $18°$ (Ernst angle), $30°$, and 200 RF pulses in order to ensure that the residual error is less than $0.0001M_0$ (see Eq. [35]). No off-resonance effects were taken into account, but this does not restrict the generality. Note that, according to Eq. [13], the values of C between π and 2π can be obtained by symmetry. At $\alpha = 10°$ the results are in good qualitative agreement with the peak structure derived from the partition method in the small flip angle regime. Indeed, high amplitudes (i.e., deviations from ideal spoiling) are found at all ψ values of the form $(K/P)(2\pi)$, and the peak height is approximately independent of K and decreases with P, provided that K/P is irreducible. For example, peaks of decreasing amplitude can be observed at $\psi = 0$ (or 2π), $\frac{1}{2}(2\pi)$, $\frac{1}{3}(2\pi)$, $\ldots$, $\frac{1}{7}(2\pi)$, and so forth. Also, peaks of equal amplitudes occur at $\psi = \frac{1}{5}(2\pi)$, and $\frac{2}{5}(2\pi)$, as well as $\psi = \frac{1}{7}(2\pi)$, $\frac{2}{7}(2\pi)$ and $\frac{3}{7}(2\pi)$. However, comparison of Figs. 3e and 4a shows that, even at $\alpha = 10°$, the small flip angle approximation tends to overestimate $|C|$. Additional simulations (results not shown) have demonstrated an improving quantitative agreement when the flip angle is decreased (e.g., less than 5% error at $\psi = \pi/2$ when $\alpha = 1°$). At larger α values, the peaks are broadened and the regular structure found in the small flip angle regime is less apparent. The peak heights increase from $\alpha = 10°$ to $\alpha = 30°$, but the quadratic dependence found in the small flip angle regime (see Eq. [20]) does not hold for these α values.

Figure 5 gives the modulus of the FLASH signal normalized to M_0, computed by means of the Fourier expansion method with the same parameters as above, and $TE = 0$. In agreement with the results of the partition method (see Eq. [24]), as well as previous numerical simulations and in vitro experiments (4–6,8), the same peak structure is found in the graph of S_{FLASH} as in the graph of C versus ψ, with peaks oriented upwards at $\alpha > \alpha_E$ and downwards at

a

b

c
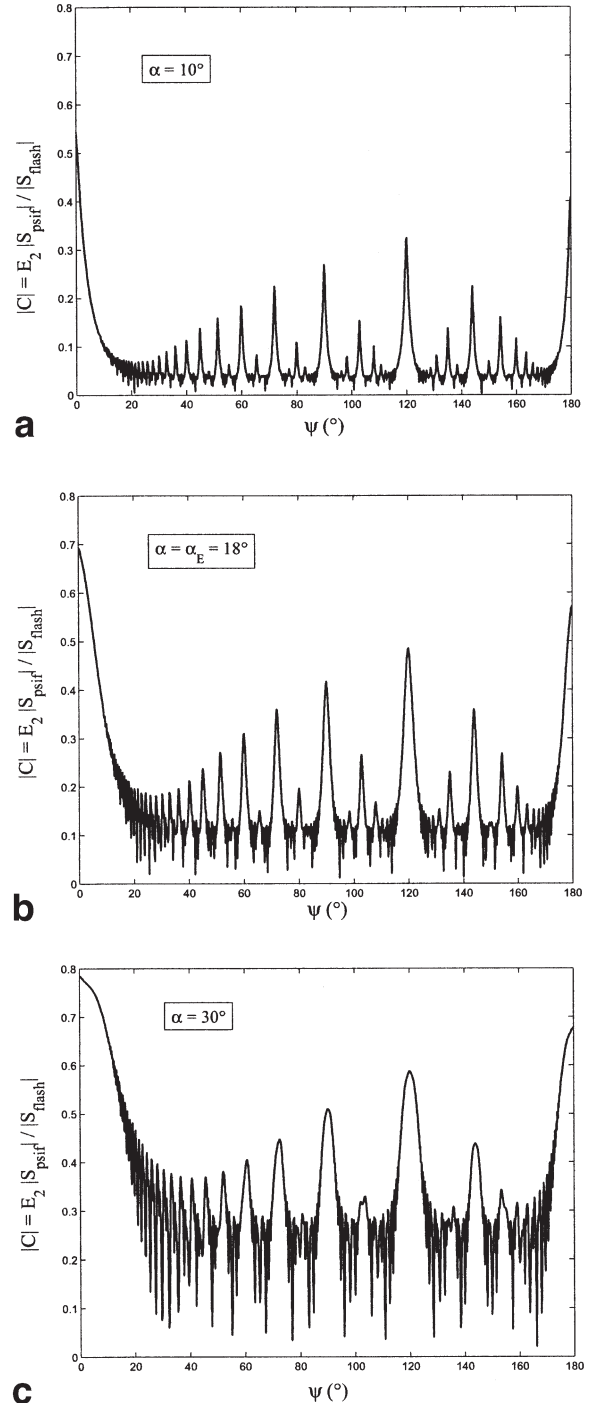
FIG. 4. "Exact" values of $|C|$, that is, E_2 times the ratio between PSIF and FLASH signal magnitudes, or equivalently the ratio between absolute values of the coherent transverse magnetization at the end and the beginning of the repetition interval. Parameter values are $\alpha = 10°$ (**a**), $18°$ (**b**) (Ernst angle), and $30°$ (**c**); $T_1/TR = 20$; $T_2 = T_1$; and ψ variable. The results are obtained by means of the Fourier expansion method with 200 repetition intervals, corresponding to a residual error smaller than $0.0001M_0$ for all magnetization components.

$\psi < \alpha_E$. At $\alpha = 10°$, ψ values far from the most intense peaks (i.e., far from ψ values of the form $(K/P)2\pi$, with P small) give rise to signal intensities close to that calculated
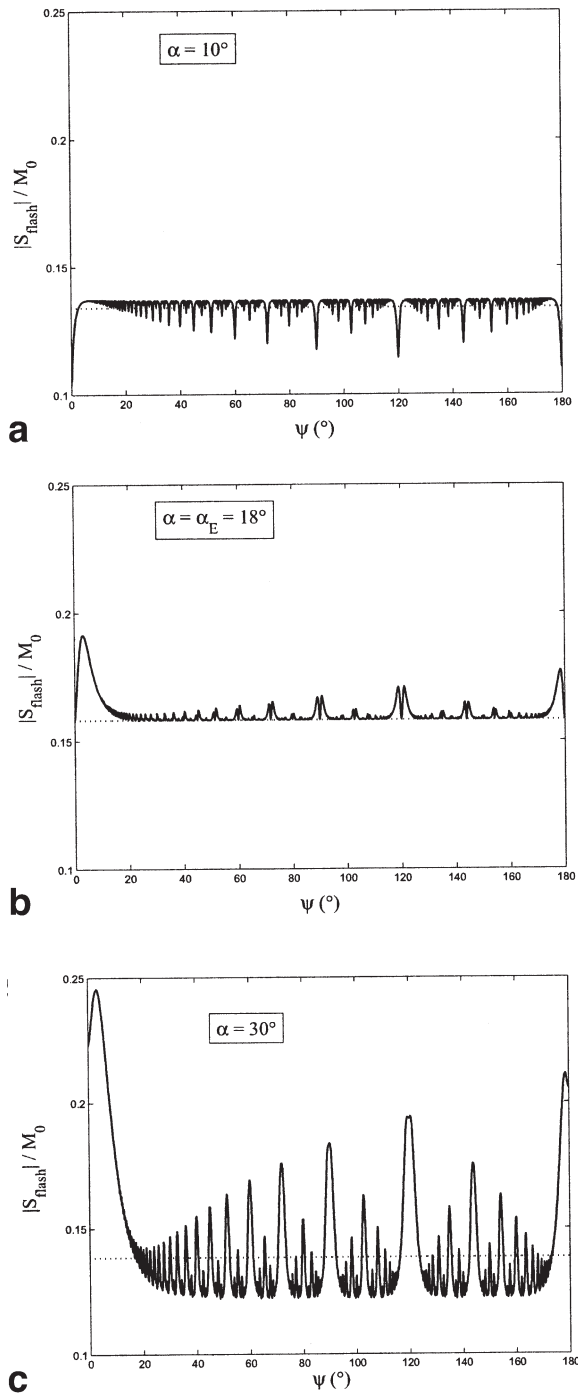
FIG. 5. Solid line: modulus of the steady-state signal intensity normalized to M_0, as a function of the phase increment ψ, for a FLASH sequence ($k = 0$) with $T_1/TR = 20$; $T_2 = T_1$; $\alpha = 10°$ (**a**), $18°$ (**b**) (Ernst angle), and $30°$ (**c**); $TE = 0$; no permanent off-resonance effects. The results are obtained by means of the Fourier expansion method with 200 repetition intervals, corresponding to a residual error smaller than $0.0001M_0$ for the magnetization components. Dotted line: ideally spoiled signal intensity (Ernst formula (1–3)). Peaks occur at $\psi = (K/P)2\pi$, with K and P integer. The peak values are local maxima at $\alpha > \alpha_E$ and local minima at $\alpha < \alpha_E$. The deviations from ideal spoiling are smallest at $\alpha = \alpha_E$.

under the hypothesis of ideal spoiling. This is in agreement with C values close to 0 at these positions along the ψ axis. At $\alpha = 30°$, the small flip angle approximation is not really valid and C remains significantly different from 0 even far from the largest peaks; consequently, the "baseline" signal is not equal to the ideal spoiling value. At $\alpha = \alpha_E$ (i.e., $18°$ in this example) the imaginary part of the complex signal (i.e., the signal in the y channel) is exactly equal to the ideally spoiled signal (see Eq. [24]), but the signal modulus deviates slightly from ideal spoiling due to non-zero values of the imaginary part of C. In the small flip angle limit, these can be attributed to the dispersion part of the peaks contributing to C (see Eq. [20] and Fig. 2).

Finally, Fig. 6 shows the ratio between echo-shifted and FLASH steady-state signal intensities, as calculated by the Fourier expansion method (solid line). At $\psi = 0$ the ratio is lower than $E_2\cos^2(\alpha)$, that is, the value that would be expected if only the primary ES pathway {1,1} contributed to the signal (dotted line). According to the results of the partition method (see above) and to Ref. (13), in the small flip angle regime this signal loss is mainly caused by the destructive interference between the primary ES pathway and secondary ES pathways of the form {1(0)$_j$1}, that is, the second order terms in α. When ψ increases, these pathways acquire different phases and cancel each other; hence, the ratio $|S_{ES-FFE}/S_{FLASH}|$ increases. At $\alpha = 10°$ this signal recovery is well described by the small flip angle formula (Eq. [28]) (dashed-dotted line): qualitative agreement with the results of the Fourier expansion method for ψ below $20°$ and quantitative agreement above $20°$. For higher flip angle values, the signal recovery with increasing ψ does still hold but is not accurately described by Eq. [28]. For all α values, the ratio between ES-FFE and FLASH signals is higher than $E_2\cos^2(\alpha/2)$ when ψ approaches $180°$.

EXPERIMENTS

Methods

All experiments were performed using a 1.5 T Philips Gyroscan Intera scanner (Best, The Netherlands) equipped with the quadrature head coil. A 1.5 l cylindrical bottle filled either with an $MnCl_2$ solution ($T_1 = 800$ ms and $T_2 = 100$ ms, similar to gray matter at 1.5 T) or with tap water ($T_1 = 2860$ ms and $T_2 = 2050$ ms, similar to CSF at 1.5 T) was placed parallel to the main magnetic field. The imaging volume was positioned at the center of the bottle, that is, in a region where field homogeneity was such that $T_2 = T_2^*$ in good approximation.

3D RF-spoiled gradient-echo sequences were implemented with FLASH ($k = 0$), PSIF ($k = -1$), and ES-FFE ($k = 1$) acquisition schemes. TR and TE were 25 ms and 9 ms, respectively. The acquisition matrix was $80 \times 40 \times 17$ with a resolution of 3.5 mm $\times$ 3.5 mm $\times$ 5 mm (frequency encoding $\times$ phase encoding $\times$ second phase encoding and slab selection direction, parallel to the main field), resulting in an acquisition time of 17 s for the full volume. The slab thickness (as determined by the RF pulse bandwidth and selection gradient) was 42.5 mm, that is, 1/2 of the encoded FOV in the second phase encoding direction, in order to avoid aliasing due to slab profile
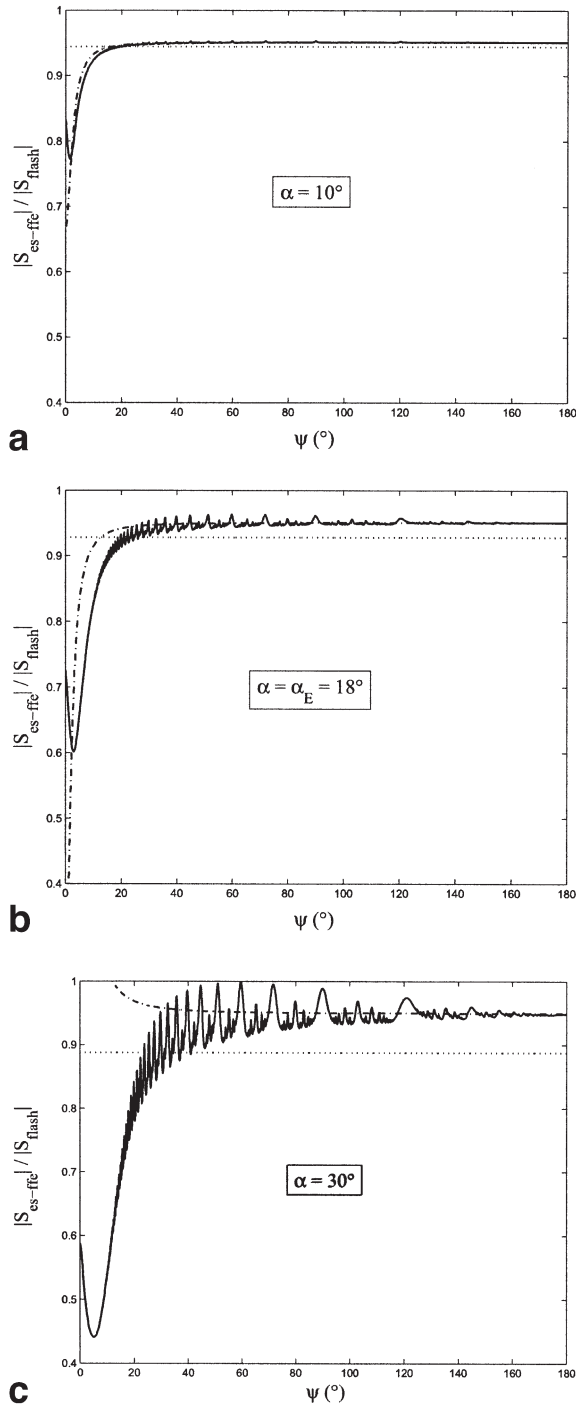
FIG. 6. Solid line: steady-state signal intensity for a spoiled echo-shifted sequence ($k = 1$) with $T_1/TR = 20$; $T_2 = T_1$; $T_2' = \infty$; ψ variable; and $\alpha = 10°$, $18°$ (Ernst angle, $\cos\alpha_E = E_1$), and $30°$; normalized to the signal intensity in the FLASH sequence with identical parameters. The results are obtained by means of the Fourier expansion method with 200 repetition intervals, corresponding to a residual error smaller than $0.0001M_0$ for the magnetization components. Dashed-dotted line: ratio found in the small flip angle approximation, that is, $E_2(TE)|1 - (\alpha^2/2)H^*(\psi)|$ (Eqs. [28] and [15]). Dotted line: ratio found by assuming that only the primary ES pathway contributes to the echo-shifted signal intensity, that is, $E_2\cos^2(\alpha/2)$.

imperfections. The bandwidth per pixel was 85 Hz. Two dummy scans were performed before recording data, in order to reach the steady-state signal intensity. In all acquisition schemes (FLASH, PSIF, and ES-FFE) the net gradient area per *TR* was such that a phase spread of 4π per *TR* occurred in all directions across each voxel. The flip angle was set successively to 5, 15, 25, 40, 60, and 80° and the phase increment ψ to 0, 72° ($= \frac{1}{5}(2\pi)$) and 117° (i.e., one of the most commonly chosen values (6)).

For both phantoms, all sequences, all flip angles, and all ψ values, the signal intensity was computed as the average of the modulus image in a region of interest located in the central slice, where the nominal flip angle was effectively obtained. The PSIF and ES-FFE signal intensities were normalized to FLASH and compared to simulations using the Fourier expansion method (no permanent off-resonance effects) with 318 pulses for the first phantom and 1134 pulses for the second one, in order to reduce the residual error to less than $0.0001M_0$.

Results

Solid lines and stars in Fig. 7 correspond to measured and simulated ratios of PSIF versus FLASH signal intensities. Plots a and d illustrate the constructive interference between refocused pathways in coherent GE sequences ($\psi = 0$), giving rise to the PSIF signal or, equivalently, coherent transverse magnetization at the end of the repetition interval. This effect increases with α ($C \div \alpha^2$ in the small flip angle approximation) and is most intense at long T_2 since the magnetization remains transverse for at least 2 *TR* intervals along all refocused pathways. Plots b and c demonstrate a significant reduction of the measured ratio $S_{\text{PSIF}}/S_{\text{FLASH}}$ by RF spoiling, in good agreement with the numerical simulations. Although $72° = \frac{1}{5}(2\pi)$ coincides with the position of a peak (see the results of numerical simulations for the ratio C), and should therefore lead to less effective spoiling, the attenuation is not stronger at $\psi = 117°$ than at $\psi = 72°$. This is due to the relatively short T_2 value ($T_2/TR = 4$), leading to a weak peak amplitude since all contributions have spent at least 10 *TR* intervals in the transverse state. With longer T_2 values (left column, plots e and f), the theory predicts a better suppression of coherent transverse magnetization at the end of the repetition interval for $\psi = 117°$ than for $\psi = 72°$, at small flip angle. However, the experimental data do not fully confirm this behavior, most probably because of the extreme sensitivity of signal intensities to any imperfection in the actual implementation of a given phase increment ψ at high T_1/TR (see our discussion of the shape of $H(\psi)$ or Fig. 7 in Ref. (6)). Note that, despite the poor quantitative agreement with numerical simulations, the PSIF signal reduction by RF spoiling is in good qualitative agreement with the expectations for both values of ψ. The ratios of ES-FFE versus FLASH signals are depicted in Fig. 7 by dashed lines (simulations) and crosses (experiment). At $\psi = 0$ (a and d), the destructive interference between primary and secondary ES pathways (13) is noticeable, particularly when α increases, leading to ratios smaller than the quantity $E_2\cos^2(\alpha/2)$, which would be obtained if only the primary ES pathway contributed. The signal recovery due to the loss of coherence of secondary ES path-
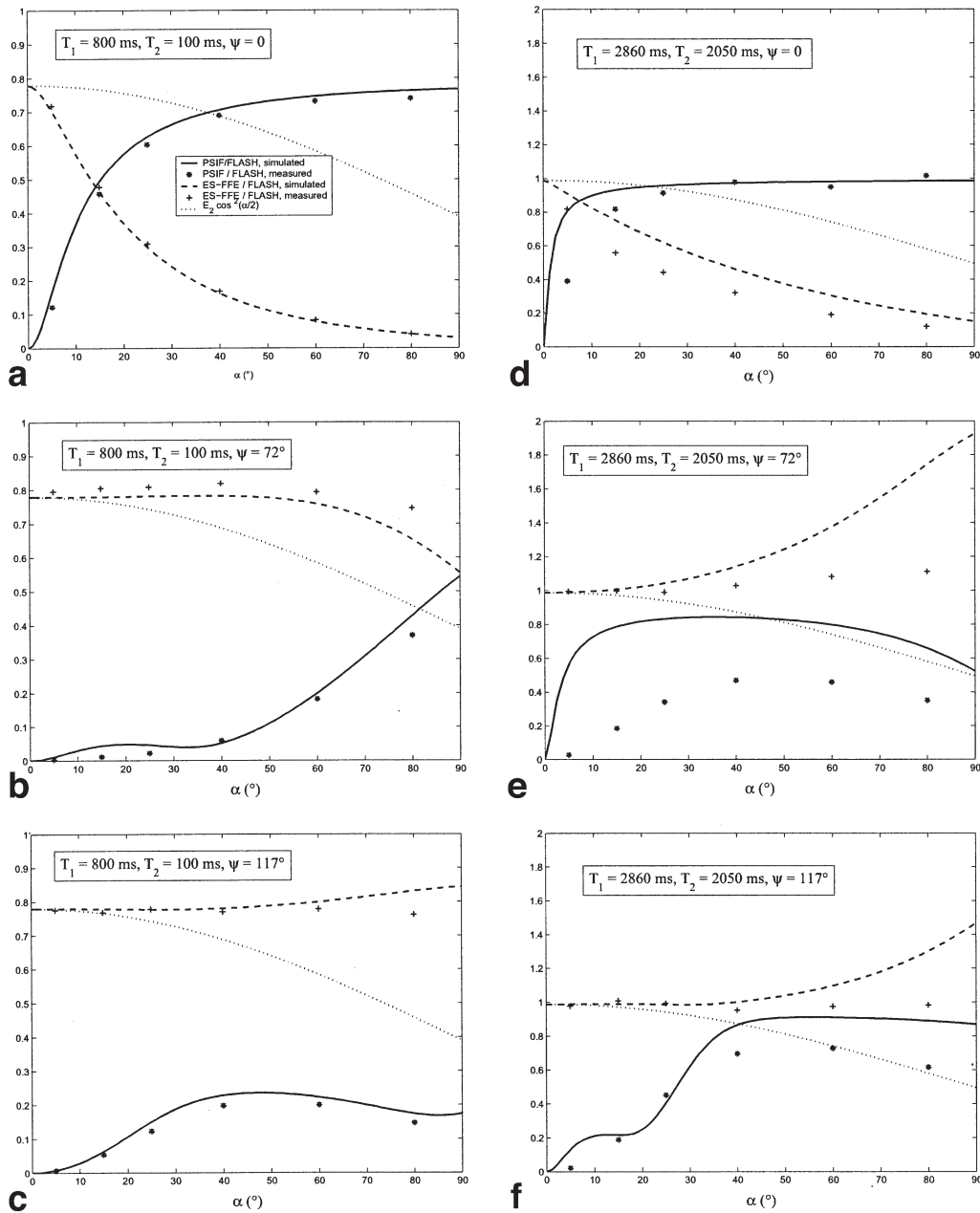
FIG. 7. Comparison of experimental measurements and numerical simulations of the ratios $|S_{PSIF}/S_{FLASH}|$ (stars, solid lines) and $|S_{ES-FFE}/S_{FLASH}|$ (crosses, dashed lines) in an MnCl$_2$ solution (left) and tap water (right) at $TR = 25$ ms, $TE = 9$ ms, $\psi = 0$ (top row), 72° (middle row), and 117° (bottom row). Numerical simulations were based on the Fourier expansion method. The former ratio illustrates the attenuation of coherent transverse magnetization at the end of the interval in RF-spoiled sequences ($\psi = 72°$, 117°) as compared to coherent sequences ($\psi = 0$), while the latter demonstrates the suppression of destructive interferences between primary and secondary ES pathways by RF spoiling in echo-shifted sequences. The agreement between simulations and experiment is excellent for the MnCl$_2$ solution ($T_1/TR = 32$, $T_2/TR = 4$) but only modest for tap water ($T_1/TR = 114$, $T_2/TR = 82$), most probably because of the extremely steep variation of signal intensities as a function of ψ for such long relaxation times. The dotted line is the ratio between ES-FFE and FLASH signal that would be expected if only the primary ES pathway contributed to the ES-FFE signal, that is, $E_2\cos^2(\alpha/2)$.

ways with RF spoiling is observed in plots b, c, e, and f, with again a better agreement between theory and experiment at shorter relaxation times. Generally speaking, the agreement between simulations and experiment tends to be poorer at high flip angle values, because all signal intensities are low and the computed ratios are sensitive to noise.

DISCUSSION AND CONCLUSIONS

In the first part of this article we have proposed a new demonstration of the property that RF-spoiled sequences, although non-periodic by nature, can be designed in such a way that the received signal reaches a stationary state. A key element of the proof was to simplify the

problem by formulating it in terms of linearly increasing precession angles instead of quadratically varying pulse phases. Another important step consisted of realizing that, while the evolution of each isochromat can be studied independently with purely algebraic methods in the coherent case, for RF-spoiled sequences it is necessary to think in terms of functions of the precession angle θ. By doing this, it was possible to show that the system converges towards a pseudo-steady state where, apart from a variable shift along the θ axis, the magnetization profile $\mathbf{M}_n^+(\theta)$ is stationary. Starting from this fundamental property, an integration over precession angles enabled us to prove that, if the net gradient surface per repetition interval is large and the detector phase set to $k\phi_{n-1}$, a steady-state signal is reached. It should be noted that the work of Sobol and Gauntt (10) already established the existence of steady-state signals for all possible coherence orders (i.e., FLASH, FISP, and ES-FFE sequences, or any higher order acquisition scheme) and could in principle also be used to derive analytical solutions for all values of the phase increment of the form $(K/P)(2\pi)$ (although the resulting expressions become very cumbersome as P increases). However, the integration method adopted here presented a number of advantages. First of all, the mathematical treatment was simpler, thereby allowing us to view the existence of a pseudo-steady state in RF-spoiled sequences as a direct application of general functional analysis results (see Appendix B). Also, this technique did not directly deal with signal intensities, but described the evolution of local magnetization vectors which were subsequently integrated to obtain the signal intensity from a whole voxel. This 2-step process had the advantage of being closer to the physical mechanism of signal formation, and allowed magnetic field inhomogeneities (or other permanent off-resonance effects) to be naturally incorporated as an additional variable in the precession angle distribution. Another fact suggested previously (6) and rigorously demonstrated here was the need for a large net gradient area per repetition interval, which actually resulted from the non-convergence of the magnetization vector for isolated isochromats. Also clarified was the detector phase modulation schemes required to eliminate signal phase variations, which would otherwise corrupt the phase encoding process. In the particular case of RF-spoiled echo-shifted sequences, this provided a mathematical justification of the heuristic argument that, in the quadratic pulse phase implementation, the n-th readout should be in-phase with the $(n-1)$-th pulse (12,16). Other benefits of the integration method were the demonstration of the symmetry with respect to $\psi = 0$ (see Eq. [13] and Appendix C) and the upper bound for the difference between the current and steady-state signal intensities (see Eq. [35] and Appendix E), which is important to assess the precision of numerical estimates of the steady-state signal and to make predictions about the properties of transient-state imaging techniques. The two latter results were, to the authors' knowledge, never proved before. Finally, it should be emphasized that the derivation of the pseudo-steady state magnetization served also as a basis for the formal development of the partition method (see Appendix D). A limitation of our approach is the fact that the linear precession angle variation (or equivalently the quadratic pulse phase

variation) was assumed from the beginning of the analysis, while Sobol and Gauntt (10) made no prior hypothesis about the type of variation of the RF pulse phase and showed that only the quadratic pattern leads to a steady-state signal.

A second important goal of this article was to gain more physical intuition about signal formation in RF-spoiled sequences by decomposing the steady-state signal into a sum of gradient, spin, and stimulated echoes, as proposed initially by Kaiser and coworkers (11). The idea of qualitatively representing the steady-state signal in gradient echo sequences as a superposition of echoes originating from previous pulses was already suggested in Ref. (29) and was used as a semi-quantitative justification of the linearly increasing precession angle in RF-spoiled sequences (3,6). However, the insight gained by these analyses remained limited by the lack of theoretical understanding of the decomposition method itself. Actually, the original article of Kaiser and colleagues (11) addressed only the coherent case ($\psi = 0$, no RF spoiling) and was "based on physical arguments rather than on a mathematical expansion." A complete mathematical justification of the method was proposed in Ref. (13) for the coherent case and has been extended here to the problem of RF-spoiled sequences formulated in terms of linearly increasing flip angles. The derivation started with a series expansion (see Eq. [14] and Appendix D) of the pseudo-steady state magnetization defined in the first part of the article, in which each term could be interpreted as a component originating from a previous RF pulse. The signal intensity of FLASH, PSIF, and echo-shifted sequences was then obtained by selecting the appropriate components in the sum. Finally, the root of the partition tree, that is, the homogeneous transverse magnetization just after each RF pulse, was derived from the sum of refocused pathways (or, equivalently, those contributing to the PSIF signal), using the relationships between homogeneous magnetization components just before and just after each RF pulse. Note that the latter step was already described in the original paper of Kaiser and coworkers (11) but was omitted in Ref. (13) since, in the coherent case, the integration method provides an analytical result for the homogeneous transverse magnetization just after the RF pulse (or, equivalently, the N-FFE signal) (13,30). By further restricting the summation to second order terms in α, that is, assuming that the flip angle is small, this approach yielded a physical interpretation of the peaks observed by several authors in the graph of FLASH signal versus precession angle increment (ψ), both with numerical simulations and in vitro experiments (4–6,8). We found that the peak observed at $\psi = (K/P)(2\pi)$ (with K and P integer, and K/P irreducible) was due to the incomplete destructive interference of several families of refocused pathways, namely $\{(1)_P(0)_j(-1)_P\}$, $\{(1)_{2P}(0)_j(-1)_{2P}\}$, $\{(1)_{3P}(0)_j(-1)_{3P}\}$, ... ($j = 0, 1, 2, 3, \ldots$), leading to non-zero values of the ratio C of PSIF and FLASH signal intensities. Through the relationships (Eqs. [24] and [25]) between this ratio and the FLASH signal, we were able to predict that these high C values yield positive or negative deviations from ideal spoiling in the FLASH signal, according to whether α is above or below the Ernst angle. Note that the semi-quantitative analysis of Duyn (8) provided another interpretation of the

position and intensity of the peaks, based on Fourier analysis and an analogy with BURST sequences. However, this approach predicted only positive peaks of height proportional to $1/\sqrt{P}$ and cannot account for negative deviations from ideal spoiling. The application of the partition method in the small flip angle regime to RF-spoiled ES-FFE sequences revealed that the destructive interference between primary and secondary ES pathways observed in coherent ES-FFE sequences (13) is suppressed for all values of ψ apart from the vicinity of $\psi = 0$. This does not, however, always imply that the ES-FFE signal intensity grows since the increase of $S_{\text{ES–FFE}}/S_{\text{FLASH}}$ is generally accompanied by a decrease of S_{FLASH}. Note also that the actual signal intensity in RF-spoiled ES-FFE sequences will generally be higher than the value

$$\frac{M_0(1 - E_1)\sin \alpha}{1 - E_1\cos \alpha} E_2(TR + TE)\cos^2 \frac{\alpha}{2}$$

assumed by Chung (12). Indeed, even if ψ is chosen to be "far" from all large peaks, such that the first factor is a good estimate of the transverse magnetization just after the pulse, the factor $\cos^2(\alpha/2)$ underestimates the resultant of all echo-shifted pathways.

The predictions of the partition method in the small flip angle limit have been compared to numerical simulations based on a Fourier expansion of the magnetization as a function of the precession angle θ. This algorithm is particularly efficient since it provides the exact signal intensities for all coherence orders (i.e., for FLASH, echo-shifted sequences, etc.) during the transient phase, and approximate values of the steady-state signals with good control over the precision of these estimates. Note also that, although meant to be used for numerical simulations, the formulas given here in the context of the Fourier expansion method are actually very similar to those used in Ref. (10) as a starting point for analytical developments. The small flip angle approximation of the ratio C was found to be in good qualitative agreement with numerical estimates, although the height and sharpness of the peaks tend to be overestimated, especially for flip angles close to or above the Ernst angle. This mismatch might be due to higher order components (α^4 or higher), which are small but numerous. The numerical simulations confirmed also the theoretical predictions that the sign of $\alpha - \alpha_{\text{E}}$ determines the peak orientation for FLASH signal intensities, and that the ratio of echo-shifted and FLASH signals increases with ψ.

The theoretical findings have been confirmed by in vitro measurements, with a better agreement between simulations and experiments for shorter relaxation times, probably because the sensitivity to small changes in ψ is much higher for long T_1 and T_2. For in vivo conditions, it is expected that effects such as flow and diffusion will impact RF-spoiled signal. These could be accounted for by introducing flow-related precession angles in the Bloch equations (8). Other extensions of the present work could study the implications of the partition method for higher coherence orders ($|k| > 1$).

APPENDIX A: EQUIVALENCE BETWEEN QUADRATIC PULSE PHASE AND LINEAR PRECESSION ANGLE VARIATIONS

Assuming a variable pulse phase φ_n and a constant precession angle θ per *TR*, the Bloch equations yield the following recurrence for the magnetization states just after RF pulses:

$$\mathbf{M}_{n+1}^+(\theta) = \mathbf{P}(\varphi_{n+1})\mathbf{R}_{x,\alpha}\mathbf{P}(-\varphi_{n+1})(\mathbf{E}(TR)\mathbf{P}(\theta)\mathbf{M}_n^+(\theta) + (1 - E_1(TR))M_0\mathbf{1}_z \quad [36]$$

with the same notations as in the main text. In a frame of reference that matches the phase of the latest RF pulse, that is, which is rotated by φ_n around the z axis with respect to the static frame (x, y, z), the observed magnetization vector is

$$\tilde{\mathbf{M}}_n^+(\theta) = \mathbf{P}(-\varphi_n)\mathbf{M}_n^+(\theta). \quad [37]$$

The recurrence for $\tilde{\mathbf{M}}_n^+(\theta)$ is

$$\tilde{\mathbf{M}}_{n+1}^+(\theta) = \mathbf{A}(\theta + \Delta\varphi_n)\tilde{\mathbf{M}}_n^+(\theta) + \mathbf{B} \quad [38]$$

where

$$\Delta\varphi_n = \varphi_n - \varphi_{n+1}. \quad [39]$$

Equation [38] is exactly the same as Eq. [2] if $\Delta\varphi_n = \phi_n = \phi_0 + n\psi$, that is, if

$$\varphi_n = \varphi_0 + \left(\frac{\psi}{2} - \phi_0\right)n - \frac{\psi}{2}\,n^2, \quad [40]$$

meaning that the magnetization vectors generated in a fixed frame of reference by an MR sequence with constant phase pulses and linearly varying precession angles can also be obtained by means of a sequence with constant precession angle and quadratic pulse phase variation, provided that the frame of reference follows the phase of RF pulses. As a consequence, the signal measured by setting the detector phase to $k\phi_{n-1}$ in the former scheme is the same as that measured with the detector phase set to $\varphi_n + k\phi_{n-1}$ in the latter. The difference between $\varphi_n + k\phi_{n-1}$ and φ_{n-k} is independent of n; hence, the detector phase modulation required in the quadratic pulse phase approach can be thought of as matching the phase of the n-th readout with the phase of pulse number $n - k$, as previously suggested in the special case of echo-shifted sequences ($k = 1$) (16).

APPENDIX B: PSEUDO-STEADY STATE IN RF-SPOILED SEQUENCES AS A CONSEQUENCE OF FUNCTIONAL ANALYSIS RESULTS

In this Appendix it is shown that the pseudo-steady state defined in the Theory section can be derived from 2 standard results of operator theory. These can be found in any textbook on functional analysis, for example, Ref. (31).

Theorem 1: Banach Fixed Point Theorem

Let $(E, \|\cdot\|)$ be a Banach space (i.e., a complete vector space with norm $\|\cdot\|$) and T a mapping of E into itself. If T is a contraction, that is, there is a constant $C < 1$ such that

$$\forall x, x' \in E : \|Tx - Tx'\| \leq C\|x - x'\|$$

then

1. T has a unique fixed point, that is, an element $\tilde{x}$ of E such that $T\tilde{x} = x$.
2. $\tilde{x}$ can be approached by iteratively applying T to any starting estimate x:
$$\forall x \in E : T^n x \rightarrow \tilde{x}.$$

3. An upper bound for the error between $\tilde{x}$ and the current approximation is given by the following inequality:
$$\forall x \in E : \|\tilde{x} - T^n x\| \leq \frac{C^n}{1 - C}\|Tx - x\|.$$

Theorem 2

Let $(E, \|\cdot\|)$ be a Banach space and $K : E \rightarrow E$ be a linear bounded operator. Let us assume that the norm of K, as defined by

$$\|K\| = \sup_{f \in E|\ \|f\| \leq 1} \|Kf\|,$$

is strictly smaller than 1. Then $(I - K)$ is invertible (I being the identity operator on E) and

$$\forall f \in E : (I - K)^{-1}f = \lim_{n \to \infty}(I + K + K^2 + \ldots + K^n)f$$

where the limit is taken with respect to the norm in E.

Application

Let us consider the Banach space $E = \{\mathbf{M}(\theta) : \mathbb{R} \rightarrow \mathbb{R}^3$ continuous and 2π periodic$\}$ with the norm

$$\|\mathbf{M}(\theta)\|_\infty = \max\left\{\|\mathbf{M}(\theta)\| = \left(\sum_{i=1}^{3} M_i(\theta)^2\right)^{1/2} \middle| \theta \in [0, 2\pi]\right\}.$$

By defining the application T as

$$T : E \rightarrow E : \mathbf{M}(\theta) \rightarrow \mathbf{A}(\theta)\mathbf{M}(\theta - \psi) + \mathbf{B}$$

one can rewrite Eq. [2] as

$$\mathbf{M}_{n+1}^+(\theta - \phi_n) = T[\mathbf{M}_n^+(\theta - \phi_{n-1})]$$

meaning that the function $\mathbf{M}_n^+(\theta - \phi_{n-1})$ can be seen as the result of $(n - 1)$ iterations of T applied to $\mathbf{M}_1^+$. T is a contraction because $\mathbf{A}(\theta)$ is the product of 2 orthogonal matrices (conserving thus euclidian distances) and 1 diagonal matrix with entries strictly smaller than 1. Therefore, by virtue of Theorem 1, the sequence $\mathbf{M}_n^+(\theta - \phi_{n-1})$ converges towards the unique fixed point of T. Translating this in equations leads directly to Eqs. [4] and [6]. Let us note that, since Theorem 1 is applied in the space E with the supremum norm, the convergence in Eq. [4] occurs in the sense of uniform convergence. The third part of Theorem 1 implies that

$$\max_{\theta \in [0, 2\pi]}\left(\|\mathbf{M}_n^+(\theta - \phi_{n-1}) - \mathbf{M}_{\text{pss}}(\theta)\|\right) \leq \frac{E_1^{n-1}}{1 - E_1}\ 3M_0.$$

By defining the operator

$$K : E \rightarrow E : \mathbf{M}(\theta) \rightarrow \mathbf{A}(\theta)\mathbf{M}(\theta - \psi)$$

on we can rewrite Eq. [6] as

$$(I - K)\mathbf{M}_{\text{pss}}(\theta) = \mathbf{B}.$$

For the same reasons as above it holds that

$$\|K\| = \sup_{\|\mathbf{M}(\theta)\|_\infty \leq 1}\|\mathbf{A}(\theta)\mathbf{M}(\theta)\|_\infty < 1.$$

Therefore, Theorem 2 can be used to solve the equation for $\mathbf{M}_{\text{pss}}(\theta)$, leading to Eq. [5]. Again, since Theorem 2 is applied in the space E with the supremum norm, the convergence in Eq. [5] occurs in the sense of uniform convergence.

APPENDIX C: PROOF OF EQ. [13]

Let $\mathbf{W}$ represent the inversion of the x magnetization component, that is, $\mathbf{W} = \text{diag}(-1, 1, 1)$. The equalities

$$\mathbf{W}^2 = \mathbf{I}, \quad \mathbf{W}\mathbf{A}(\theta)\mathbf{W} = \mathbf{A}(-\theta), \quad \mathbf{W}\mathbf{B} = \mathbf{B}, \quad \mathbf{W}\mathbf{P}(\theta)\mathbf{W} = \mathbf{P}(-\theta),$$

together with Eq. [5], imply that

$$\langle\mathbf{P}(-k\theta)\mathbf{M}_{\text{pss}}(\theta; -\psi)\rangle = \langle\mathbf{P}(-k\theta)[\mathbf{I}$$
$$+ \mathbf{A}(\theta) + \mathbf{A}(\theta)\mathbf{A}(\theta + \psi) + \ldots]\mathbf{B}\rangle$$
$$= \langle\mathbf{P}(k\theta)[\mathbf{I} + \mathbf{A}(-\theta) + \mathbf{A}(-\theta)\mathbf{A}(-\theta + \psi) + \ldots]\mathbf{B}\rangle$$
$$= \mathbf{W}\langle\mathbf{P}(-k\theta)[\mathbf{I} + \mathbf{A}(\theta) + \mathbf{A}(\theta)\mathbf{A}(\theta - \psi) + \ldots]\mathbf{B}\rangle$$
$$= \mathbf{W}\langle\mathbf{P}(-k\theta)\mathbf{M}_{\text{pss}}(\theta; \psi)\rangle.$$

By using the complex notation of transverse magnetization, this can be rewritten as

$$\langle e^{-ik\theta}M_{\text{T,pss}}(\theta; -\psi)\rangle = -\langle e^{-ik\theta}M_{\text{T,pss}}(\theta; \psi)\rangle^*.$$

This, together with the expression of the steady-state signal intensity (see Eq. [12]) proves the announced result.

APPENDIX D: PARTITIONING THE PSEUDO-STEADY STATE MAGNETIZATION

The partition method is based on the following decomposition of the pseudo-steady state magnetization:

$$\mathbf{M}_{pss}(\theta) = \sum_{\ell=1}^{\infty} \boldsymbol{\mu}_{pss,\ell}(\theta) \qquad [41]$$

where

$$\boldsymbol{\mu}_{pss,1} = \langle \mathbf{M}_{pss}(\theta) \rangle$$

$$\boldsymbol{\mu}_{pss,\ell+1}(\theta) = \mathbf{A}(\theta)\boldsymbol{\mu}_{pss,\ell}(\theta - \psi) - \langle \mathbf{A}(\theta)\boldsymbol{\mu}_{pss,\ell}(\theta - \psi) \rangle.$$

This equality is an extension of the series expansion presented in Ref. (13) for the coherent case and is proved in a similar way, using the pseudo-steady state equation (Eq. [6]) instead of the steady-state equation (Eq. [8]). Due to the relationship (Eq. [7]) between the magnetization states $\mathbf{M}_n^+(\theta)$ and the function $\mathbf{M}_{pss}(\theta)$ in the pseudo-steady state ($n \to \infty$), the decomposition can be rewritten as

$$\mathbf{M}_n^+(\theta) = \sum_{\ell=1}^{\infty} \boldsymbol{\mu}_{n,\ell}(\theta) \qquad [42]$$

with

$$\boldsymbol{\mu}_{n,\ell}(\theta) = \boldsymbol{\mu}_{pss,\ell}(\theta + \phi_{n-1}).$$

For these new components the recurrence becomes

$$\boldsymbol{\mu}_{n,1} = \langle \mathbf{M}_{pss}(\theta) \rangle$$

$$\boldsymbol{\mu}_{n,\ell+1}(\theta) = \mathbf{A}(\theta + \phi_{n-1})\boldsymbol{\mu}_{n-1,\ell}(\theta)$$
$$- \langle \mathbf{A}(\theta + \phi_{n-1})\boldsymbol{\mu}_{n-1,\ell}(\theta) \rangle. \qquad [43]$$

The second step of the partition method consists of separating longitudinal and transverse magnetization components at each step of the recurrence, that is, further decomposing each term of Eq. [42] to obtain the series expansion (Eq. [14]) described in the main text. Like in the coherent case (13), this is achieved by expressing Eq. [43] in the coordinate system (M_T, M_T^*, M_z) and splitting RF pulses into a 0°, a 90°, and a 180° component. The generation of longitudinal and 2 transverse components from a transverse component is then described by:

$$\mu_{n,\{q_1...q_{\ell-1}\pm 1\pm 1\}}(\theta) = \cos^2 \frac{\alpha}{2} E_2 e^{i(\theta+\phi_{n-1})} \mu_{n-1,\{q_1...q_{\ell-1}\pm 1\}}(\theta) \qquad [44]$$

$$\mu_{n,\{q_1...q_{\ell-1}\pm 10\}}(\theta) = \sin \alpha E_2 e^{i(\theta+\phi_{n-1})} \mu_{n-1,\{q_1...q_{\ell-1}\pm 1\}}(\theta) \qquad [45]$$

$$\mu_{n,\{q_1...q_{\ell-1}\pm 1\mp 1\}}(\theta) = \sin^2 \frac{\alpha}{2} E_2 e^{-i(\theta+\phi_{n-1})} \mu_{n-1,\{q_1...q_{\ell-1}\pm 1\}}^*(\theta) \qquad [46]$$

where the physical longitudinal magnetization associated with component $\{q_1 \dots q_\ell 0\}$ is given by the imaginary part of $\mu_{q_1...q_\ell 0}$. For an initially longitudinal component, one obtains

$$\mu_{n,\{q_1...q_{\ell-j-1}\pm 1(0)j\pm 1\}}(\theta) = -\frac{1}{2} \sin \alpha E_1 \mu_{n-1,\{q_1...q_{\ell-j-1}\pm 1(0)j\}}(\theta) \qquad [47]$$

$$\mu_{n,\{q_1...q_{\ell-j-1}\pm 1(0)j 0\}}(\theta) = \cos \alpha E_1 \mu_{n-1,\{q_1...q_{\ell-j-1}\pm 1(0)k\}}(\theta) \qquad [48]$$

$$\mu_{n,\{q_1...q_{\ell-j-1}\pm 1(0)j\mp 1\}}(\theta) = \frac{1}{2} \sin \alpha E_1 \mu_{n-1,\{q_1...q_{\ell-j-1}\pm 1(0)j\}}^*(\theta). \qquad [49]$$

In principle, both the transverse and longitudinal parts of $\langle \mathbf{M}_{pss}(\theta) \rangle$, that is, $\mu_{n,1}(\theta) = \langle M_{T,pss}(\theta) \rangle$ and $\mu_{n,0}(\theta) = \langle M_{z,pss}(\theta) \rangle$, should be considered at the root of the partition tree. However, the latter component gives rise to a pathway that is stopped after just 1 repetition interval (as a consequence of subtracting the homogeneous component at each step); hence, only the former is relevant to study signal intensities, that is, transverse magnetization.

APPENDIX E: PRECISION OF NUMERICAL ESTIMATES OF THE STEADY-STATE SIGNAL

An upper bound of the difference between current and steady-state signals is obtained as follows

$$|S_{k,n} - S_{k,ss}| \le E_2(TE)|\langle M_{T,n}^+(\theta - \phi_{n-1}) - M_{T,pss}(\theta) \rangle|$$

$$\le E_2(TE)\langle \|\mathbf{M}_n^+(\theta - \phi_{n-1}) - \mathbf{M}_{pss}(\theta)\| \rangle$$

$$\le E_2(TE)(E_1^{n-1}\|\mathbf{M}_1^+\| + (E_1^{n-1} + E_1^n + E_1^{n+1} + \dots)\|\mathbf{B}\|)$$

$$\le E_2(TE)2E_1^{n-1}M_0$$

where use has been made of Eqs. [3], [5], [11], [12], $\|\mathbf{M}_1^+\| \le M_0$, and $\|\mathbf{B}\| = (1 - E_1)M_0$. Consequently, the precision of $S_{k,n}$ as an estimate of $S_{k,ss}$ is better than $\epsilon \cdot M_0$ if

$$2E_2(TE)E_1^{n-1} \le \epsilon \qquad [50]$$

which holds if n is larger than the value given by Eq. [35]. Note that another upper bound for $\langle \|\mathbf{M}_n^+(\theta - \phi_{n-1}) - \mathbf{M}_{pss}(\theta)\| \rangle$, that is, $3M_0 E_1^{n-1}/(1 - E_1)$, could be derived directly from the Banach Fixed Point Theorem (see Appendix B). However, this quantity is larger than the upper bound derived here from the explicit expression of $\mathbf{M}_{pss}(\theta)$, and would, therefore, tend to overestimate the number of steps required to achieve a given precision.

REFERENCES

1. Ernst RR, Bodenhausen G, Wokaun A. Principles of nuclear magnetic resonance in one and two dimensions. Oxford: Clarendon; 1987.
2. Vlaardingerbroek MT, Den Boer JA. Magnetic resonance imaging. 2nd ed. Berlin: Springer-Verlag; 1999.
3. Haacke EM, Brown RW, Thompson MR, Venkatesan R. Magnetic resonance imaging, physical principles and sequence design. New York: Wiley; 1999, p 914.
4. Crawley AP, Wood ML, Henkelman RM. Elimination of transverse coherences in FLASH MRI. Magn Reson Med 1988;8;248–260.
5. Sekihara K. Steady-state magnetizations in rapid NMR imaging using small flip angles and short repetition intervals. IEEE Trans Med Im 1987;6:157–164.
6. Zur Y, Wood ML, Neuringer LJ. Spoiling of transverse magnetization in steady-state sequences. Magn Reson Med 1991;21:251–263.
7. Epstein FH, Mugler JP, Brookerman JR. Spoiling of transverse magnetization in gradient echo (GRE) imaging during the approach to steady state. Magn Reson Med 1996;35:237–245.
8. Duyn JH. Steady state effects in fast gradient echo magnetic resonance imaging. Magn Reson Med 1997;37:559–568.
9. Scheffler K. A pictorial description of steady-states in rapid magnetic resonance imaging. Concepts in Magnetic Resonance 1999;11:291–304.
10. Sobol WT, Gauntt DM. On the stationary states in gradient echo imaging. J Magn Reson Imaging 1996;6:384–398.
11. Kaiser R, Bartholdi E, Ernst RR. Diffusion and field-gradient effects in NMR Fourier spectroscopy. J Chem Phys 1974;60:2966–2979.
12. Chung YC, Duerk JL. Signal formation in echo-shifted sequences. Magn Reson Med 1999;42:864–875.
13. Denolin V, Metens T. On the calculation and interpretation of signal intensity in echo-shifted sequences. Magn Reson Med 2004;51:123–134.
14. Hennig J. Echoes—How to generate, recognize, use or avoid them in MR-imaging sequences. Part I: Fundamental and not so fundamental properties of spin echoes. Concepts in Magnetic Resonance 1991;3:125–143.
15. Gyngell ML. The Application of SSFP in rapid 2DFT NMR imaging, FAST and CE-FAST sequences. Magn Reson Imaging 1988;6:415–419.
16. Duyn JH, Mattay VS, Sexton RH, Sobering GS, Barrios FA, Liu G, Frank JA, Weinberger DR, Moonen CT. 3-Dimensional functional imaging of human brain using echo-shifted FLASH MRI. Magn Reson Med 1994; 32:150–155.
17. Van Gelderen P, Ramsey NR, Liu G, Duyn JH, Frank JA, Weinberger DR, Moonen CTW. Three-dimensional functional magnetic resonance imaging of human brain on a clinical 1.5-T scanner. Proc Natl Acad Sci USA 1995;92:6906–6910.
18. Redpath TW, Jones RA. FADE—A new fast imaging sequence. Magn Reson Med 1988;6:224–234.
19. Bruder H, Fischer H, Graumann R, Deimling M. A new steady state imaging sequence for simultaneous acquisition of two different MR images with clearly different contrasts. Magn Reson Med 1988;7:35–42.
20. Lee SY, Cho H. Fast SSFP gradient echo sequence for simultaneous acquisitions of FID and echo signals. Magn Reson Med 1988;8:142–150.
21. Kim DJ, Cho ZH. Analysis of higher order echoes in SSFP. Magn Reson Med 1991;19:20–30.
22. Arfken G. Mathematical methods for physicists. 3rd ed. Orlando, FL: Academic Press; 1985.
23. Ernst RR, Anderson WA. Application of Fourier transform spectroscopy to magnetic resonance. Rev Sci Instrum 1966;37:93–102.
24. Hargreaves BA, Vasanawala SS, Pauly JM, Nishimura DG. Characterization and reduction of the transient response in steady-state MR imaging. Magn Reson Med 2001;46:149–158.
25. Vasanawala SS, Pauly JM, Nishimura DG. Fluctuating equilibrium MRI. Magn Reson Med 1999;42:876–883.
26. Overall WR, Conolly SM, Nishimura DG, Hu BS. Oscillating dual-equilibrium steady-state angiography. Magn Reson Med 2002;47:513–522.
27. Denolin V, Metens T. Three-dimensional BOLD fMRI with spin-echo characteristics using T_2 magnetization preparation and echo-planar readouts. Magn Reson Med 2003;50:132–144.
28. Hardy GH, Wright EM. An introduction to the theory of numbers. 5th ed. Oxford, England: Clarendon Press; 1979.
29. Hennig J. Echoes—How to generate, recognize, use or avoid them in MR-imaging sequences. Part II: Echoes in imaging sequences. Concepts in Magnetic Resonance 1991;3:179–192.
30. Buxton RB, Fisel CR, Chien D, Brady TJ. Signal intensity in fast NMR imaging with short repetition times. J Magn Reson 1989;83:576–585.
31. Rudin W. Functional analysis. 2nd ed. New York: McGraw Hill; 1991.